Marine Pollution Bulletin 230 (2026) 119899

Contents lists available at ScienceDirect

Marine Pollution Bulletin

journal homepage: www.elsevier.com/locate/marpolbul

Land-use impacts on Amazon and Atlantic rainforest coastal ecosystems revealed by multiple biogeochemical markers

Échily Sartori [a,*], Cristiane dos Santos Vergilio [b], Tassiana S.G. Serafim [c], Diego Lacerda [a], Luiza Silva do Nascimento [a], Pedro Vianna Gatts [a], Mariana Freitas [a], Jamile Tamer Nasser [d], Marcelo Gomes de Almeida [a], César C. Martins [d], Nils E. Asp [e], Carlos Eduardo de Rezende [a,*]

[a] Grupo de Pesquisa em Biogeoquímica de Ecossistemas Aquáticos, Laboratório de Ciências Ambientais, Centro de Biociências e Biotecnologia, Universidade Estadual do Norte Fluminense Darcy Ribeiro (UENF), Avenida Alberto Lamego, 2000, Parque Califórnia, Campos dos Goytacazes, Rio de Janeiro, 28013-602, Brazil
[b] Laboratório de Ecotoxicologia, Departamento de Biologia, Centro de Ciências Exatas Naturais e da Saúde, Universidade Federal do Espírito Santo – Campus Alegre (UFES), Alto Universitário, S/N, Alegre, Espírito Santo, 29500-000, Brazil
[c] Leibniz Institute for Baltic Sea Research Warnemünde (IOW), Seestra�e 15, 18119, Rostock, Germany
[d] Laboratório de Química Orgânica Marinha, Instituto Oceanográfico, Universidade de São Paulo (USP), Praça do Oceanográfico, 191, Cidade Universitária, São Paulo, 05508-120, Brazil
[e] Instituto de Estudos Costeiros, Universidade Federal do Pará (UFPA), Alam, Leandro Ribeiro, S/N, Bairro Aldeia, Campus UFPA, Bragança, Pará, 68600-000, Brazil

ARTICLE INFO

Keywords:
Caeté River
Mangrove
Paraíba do Sul River
PAH
POP
Stable isotopes

ABSTRACT

Land-use changes were assessed using isotopic and elemental composition of organic matter (OM) and organic pollutants in estuarine sediments from two Brazilian basins: the Caeté River (CR, Amazon Rainforest) and the Paraíba do Sul River (PSR, Atlantic Rainforest). Between 1985 and 2024, anthropogenic land use in CR increased in 39%, while PSR decreased by 2.6%. CR sediments exhibited lower $\delta^{13}C_{org}$ (−27.3 ± 0.9‰) and $\delta^{15}N_{total}$ (2.1 ± 2.2‰) than PSR (−23.6 ± 2.9‰ and 5.6 ± 1.0‰, respectively). Seasonal variability occurred only in CR, with more ^{13}C-depleted and ^{15}N-enriched values in the rainy season, suggesting surface runoff of C_3-derived OM from rainforest or mangroves and upstream anthropogenic inputs. The Bayesian mixing model (MixSIAR) indicated clear contrasts in OM sources between basins. In the CR basin, sedimentary OM was predominantly derived from mangroves (median = 0.76), with a secondary contribution from sewage (0.18). In contrast, in the PSR basin, sewage was the dominant OM source (0.65), followed by mangrove contributions (0.28). Organic pollutants correlated with OC, showing that contaminant distribution is partly governed by OM dynamics. PAH diagnostic ratios revealed the sewage, biomass/coal burning as the main source in PSR, with additional fossil-fuel inputs, while CR reflected mixed combustion sources linked to agricultural fires and boat traffic. Organochlorine patterns in CR suggest historical pesticide use and diffuse atmospheric input, while PSR shows lindane and local/industrial influences. These results highlight contrasting OM dynamics under different land-use intensities and the dual role of estuaries in storing carbon and pollutants.

1. Introduction

Brazil hosts the world's largest area of native tropical forests (Turubanova et al., 2018), and the second largest mangrove (Bunting et al., 2022). These ecosystems regulate climate, sequester carbon, maintain hydrological balance, and shelter biodiversity (Pinto et al., 2023). However, land-use expansion, mainly livestock, has intensified deforestation, replacing native vegetation with agriculture, pasture, and secondary forests, placing Brazil among the nations with greatest tropical forest loss (Lapola et al., 2014; Pinto et al., 2023).

The Amazon and Atlantic Rainforests hold global importance but differ in conservation status (Pinto et al., 2023). The Atlantic retains only 12% of its original cover, now fragmented (Lapola et al., 2014), while the Amazon still harbors the largest continuous tropical forest, crucial for global climate regulation, though deforestation has surged from livestock, logging, mining, and urbanization (Lapola et al., 2014). Both biomes are highly biodiverse, but the Atlantic shows greater endemism (Broggio et al., 2024) and illustrates potential future

* Corresponding authors.
E-mail addresses: echilysartori1@gmail.com (É. Sartori), crezende@uenf.br (C.E. de Rezende).

https://doi.org/10.1016/j.marpolbul.2026.119899
Received 7 January 2026; Received in revised form 18 March 2026; Accepted 16 May 2026
Available online 19 May 2026

scenarios for the Amazon under similar pressures.

Replacing native forests with pastures alters soil C and N stocks, increases erosion and runoff, and mobilizes organic matter (OM) toward river systems (Serafim et al., 2023; Dow et al., 2024). During transport, OM is transformed through leaching, mineral associations, photochemical alteration, and microbial degradation, processes that preferentially mineralize labile, nutrient-rich compounds and enrich the remaining pool in refractory material and heavier isotopes (Ward et al., 2017; Bianchi et al., 2018). The preservation of these isotopic signatures is further modulated by sediment granulometry, where fine-grained fractions promote mineral-organic associations that protect OM from rapid mineralization (Keil and Mayer, 2014). Stable isotopes ($\delta^{13}C_{org}$ and $\delta^{15}N_{total}$) and the $(C:N)_a$ are widely used to trace these sources and transformation pathways. Native tropical forests dominated by C_3-plants, show lower $\delta^{13}C_{org}$ values (−32.0 to −28.6‰) and moderate $\delta^{15}N_{total}$ (4.4 to 7.7‰) (Ometto et al., 2006; Ribas, 2012; Martinelli et al., 2020), whereas land-use change alters OM composition (Bernardes et al., 2004). While $\delta^{13}C_{org}$ mainly reflects vegetation type, $\delta^{15}N_{total}$ is more sensitive to land-use practices (Lizaga et al., 2021; Vezzone et al., 2021; Park et al., 2023). Pastures and croplands dominated by C_4-plants display higher $\delta^{13}C$ values (−15 to −10‰) (Bouillon et al., 2011; Ribas, 2012), while manure and sewage inputs enrich $\delta^{15}N$ through nitrification and denitrification (Li et al., 2023). In aquatic systems, terrestrial OM mixes with autochthonous and mangrove-C3 inputs, forming isotopic gradients along the land–ocean continuum (Thornton and McManus, 1994; Serafim et al., 2023).

Estuaries, transitional zones between land and sea, retain, transform, and export OM via remineralization, photodegradation, flocculation, and sorption, preserving refractory fractions (Eisma et al., 1994; Lämmle et al., 2022; Serafim et al., 2023). Their sediments reflect combined terrestrial, anthropogenic, and marine inputs. Within estuarine systems, mangroves act as biogeochemical hotspots with large carbon stocks, intense OM cycling, and export of OM (Bouillon et al., 2008; Santos-Andrade et al., 2021; Zhao et al., 2024).

Molecular markers complement isotopic tracers by identifying anthropogenic inputs. Polycyclic aromatic hydrocarbons (PAHs) indicate contributions from sewage, biomass and fossil-fuel burning, and petroleum sources (Nam et al., 2008; Martins et al., 2010; Gurgatz et al., 2023). Persistent organic pollutants (POPs) such as the pesticides hexachlorocyclohexane (HCH) and dichlorodiphenyltrichloroethane (DDT), as well as the industrial chemical compounds polychlorinated biphenyls (PCBs), trace agricultural and urban-industrial runoff, respectively (Nam et al., 2008; Oliveira et al., 2016; Mao et al., 2021). Their hydrophobicity promotes strong adsorption to OM, coupling their transport and accumulation to the same processes controlling OM export from drainage basins to estuarine sediments (Cornelissen et al., 2005; Bianchi et al., 2018). Thus, changes in land use simultaneously affect (i) the sources and isotopic composition of OM and (ii) the type and magnitude of contaminant inputs, linking both proxies to common watershed-scale processes. Interpreted together with land-use trajectories, these complementary proxies provide a framework to investigate how human activities influence both OM dynamics and contaminant accumulation in estuarine sediments.

Despite extensive research on tropical estuaries, most studies have addressed either OM sources using stable isotopes or contaminant distributions using molecular markers, rarely integrating both approaches. This limitation constrains the understanding of how long-term land-use trajectories influence the coupled dynamics of OM composition and pollutant accumulation in estuarine sediments. Here, we investigate land-use and cover changes (1985–2024) in two contrasting Brazilian basins within the Amazon and Atlantic Rainforests and evaluate their influence on $\delta^{13}C_{org}$, $\delta^{15}N_{total}$, $(C:N)_a$, PAHs and POPs in estuarine sediments and mangrove soils along the land–ocean continuum. We hypothesize that basins with contrasting land-use histories will exhibit coherent shifts between isotopic signatures and contaminant profiles, reflecting the joint control of vegetation change, anthropogenic emissions, and OM-associated transport processes.

2. Material and methods

2.1. Amazon hydrographic basin

Located in northeastern Pará State, the Caeté River (CR) basin represents the Amazonian system investigated in this study, covering ~2230 km^2 with a 149 km main channel flowing from its headwaters in Bonito to the Caeté-Urumajó Bay. Part of the basin lies within the Caeté-Taperaçu Marine Extractive Reserve (RESEX) and includes seven municipalities and 19 traditional communities (Abdala et al., 2012; Gomes et al., 2013; Asp et al., 2018; Pereira et al., 2021).

The CR basin exhibits a markedly seasonal climate, with rainfall concentrated in the first half of the year and a pronounced dry period in the last quarter. According to the Instituto Chico Mendes de Conservação da Biodiversidade (ICMBio), average annual precipitation is 2755 mm, with a dry season in October–November (near zero rainfall), and a rainy season from December to August, peaking in March. The CR shows a mean discharge of ~50 $m^3\ s^{-1}$, ranging from 7 $m^3\ s^{-1}$ in November to 90 $m^3\ s^{-1}$, usually in April (Asp et al., 2018). Although other studies delimit the seasons slightly differently (Dittmar et al., 2001; Gomes et al., 2013), they all agree on high annual rainfall and a strongly seasonal hydrological regime. The system is macro-tidal, with spring tides about 5 m (Dittmar et al., 2001; Asp et al., 2018).

Although sparsely populated, the basin faces socio-environmental challenges due to inadequate sanitation and resource exploitation encouraged since the 1970s. Issues include open solid-waste disposal, lack of sewage treatment, and pressures from agro-industrial, logging, mining, and fishing activities (Gorayeb et al., 2009, 2011; Guimarães, 2011).

2.2. Atlantic Rainforest hydrographic basin

The Paraíba do Sul River (PSR) basin is in southeastern Brazil, the country's most densely populated and industrialized region. It covers approximately 56,927 km^2, with the main river extending 1100 km from the confluence of the Paraibuna and Paraitinga Rivers to its mouth in São João da Barra, Rio de Janeiro State (Dittmar et al., 2012; Serafim et al., 2023). The basin supplies water to several urban centers (ANA, 2011). The climate is strongly seasonal, with dry period from April to early October and rainy period from late October to March, with average river discharge ranging from 200 to 2600 $m^3\ s^{-1}$ (Marques et al., 2017; Cotovicz et al., 2020; Neves and Vilanova, 2021; Serafim et al., 2023). Although studies delimit the dry and rainy seasons differently, they all agree that the region exhibits a strong seasonal climate.

The PSR basin is heavily impacted by industrial effluents and untreated domestic sewage (Pfeiffer et al., 1986; AGEVAP, 2020). Intensive agriculture and livestock production also contribute to environmental pressures, historically including the use of organomercury-based fungicide, which have increased mercury and other metal loads. The basin has additionally experienced several environmental accidents involving industrial spills and contaminant releases (Álvarez and Valpassos, 2023). More recently, reports of illegal gold mining have introduced additional mercury inputs to the system (Gomes et al., 2022).

2.3. Field sampling

Surface sediment and soil samples from estuarine/coastal and mangrove areas were collected in the PSR (Atlantic Rainforest) and CR (Amazon Rainforest) basins between 2022 and 2023, during both dry and rainy seasons, totaling 54 samples (Fig. 1). Half were obtained along a salinity gradient (0–36 PSU), and the remainder from adjacent mangrove areas (Table S1). Samples were transported in thermal boxes and frozen at −20 °C upon arrival for analysis.

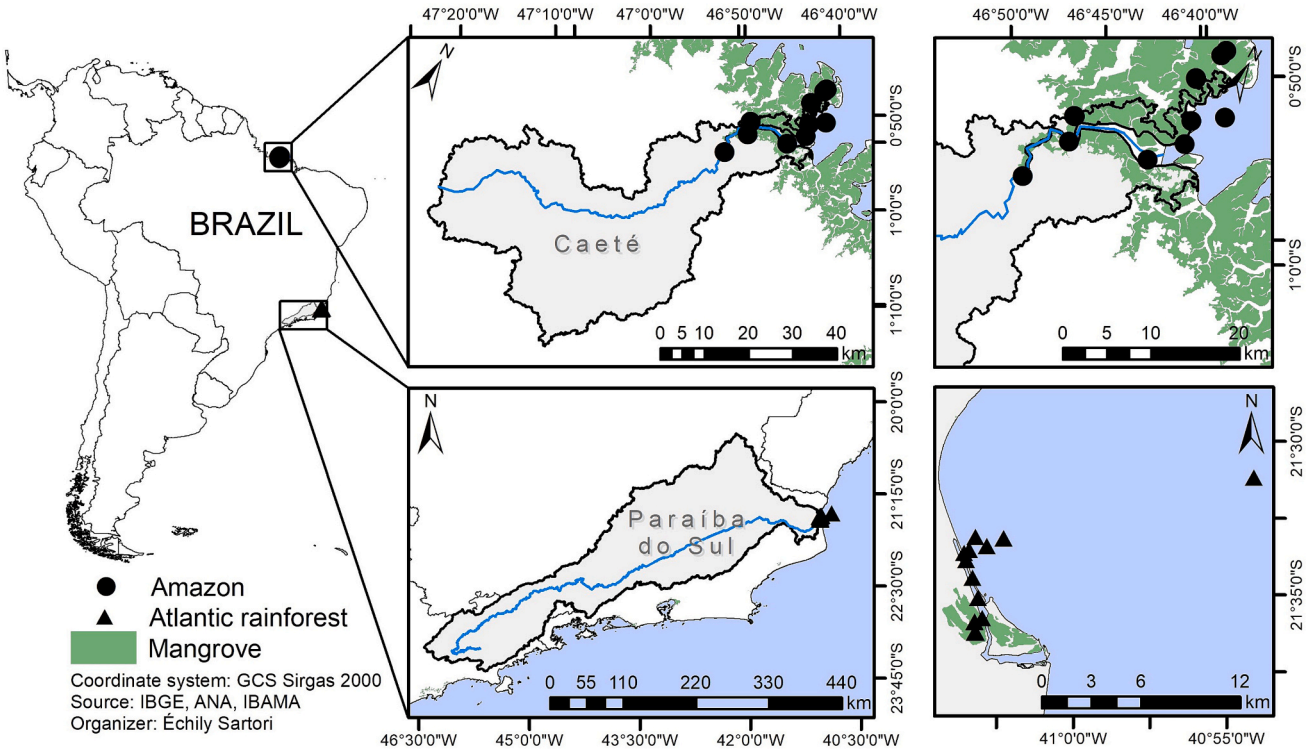

Fig. 1. Location of sediment and soil sampling sites at Caeté River (Northern Brazil, Amazon Rainforest) and Paraíba do Sul River (Southeastern Brazil, Atlantic Rainforest) estuaries.

2.4. Laboratory analysis

Samples were sieved to <2.0 mm and homogenized for elemental and stable isotope analysis following Sartori et al. (2023). Ten mg of each sample were weighed in tin capsules for TN and $\delta^{15}N_{total}$, and in silver capsules (after decarbonation with 2 mol L^{-1} HCl and drying at 110 °C) for OC and $\delta^{13}C_{org}$. The analysis was performed using an elemental analyzer (Flash 2000) connected to a mass spectrometer (Delta V Advantage, Thermo Scientific) via a CONFLO IV interface. Quantification employed acetanilide standards, with ~97% inter-replicate precision. OC and TN contents were expressed as percentages (detection limits: 0.05% and 0.02%, respectively). $\delta^{13}C_{org}$ and $\delta^{15}N_{total}$ values were expressed in ‰ relative to PDB and atmospheric N, with analytical precision of 0.1‰.

For organic contaminants (PAHs, PCBs, PBDEs, and OCPs), extraction and analysis followed Santos et al. (2020). Briefly, 15 g of freeze-dried sediment were processed, and target compounds were identified and quantified by GC–MS/MS in MRM mode. Calibration was based on certified standards. Quantification limits (QLs) corresponded to the lowest calibration levels (0.002 ng g^{-1} for OCPs, 0.001 ng g^{-1} for PCBs, and 0.006 ng g^{-1} for PAHs), and concentrations below these limits were excluded. QA/QC procedures included blanks (no interferences detected), surrogate recoveries (50–110%), spiked blanks and samples (50–110%), and certified reference material (IAEA-417), with measured concentrations within 60–90% (PAHs) and 75–90% (PCBs/OCPs) of certified values. The list of compounds analyzed and detailed information are provided in Table S2 and Fig. S2.

To evaluate the sources for PAH compounds, the diagnostics ratios were plotted to detect combustion-derived PAH following Yunker et al. (2002) and Martins et al. (2010). The combined Fl/Fl + Py (Fl: Fluoranthene; Py: Pyrene) and IP/IP + Bghi (IP: Indeno[123 *cd*]pyrene; Bghi: Benzo[*ghi*]perylene) ratios help distinguish between petrogenic, petroleum combustion and biomass combustion: 0.2–0.4 indicates petroleum dominance; 0.4–0.5 petroleum combustion; and > 0.5 sewage and/or biomass/coal combustion. Ratios of HCH isomers and DDT were used to evaluate historical pesticide use. PCB congeners were grouped according to IUPAC classification to differentiate regional atmospheric deposition from industrial or local sources.

2.5. Land use analysis

Land use and land cover data were obtained from the MapBiomas database (https://plataforma.brasil.mapbiomas.org), which provides annual land use maps for Brazil at 30 m spatial resolution from e to 2024. Basin shapefiles were used to extract the area (km^2) occupied by each land-use class for each year. The proportional area (%) of each category was then calculated relative to the total basin area (Tables S4 and S5). Full numerical precision is provided in the supplementary tables. Changes are expressed as percentage points relative to the total basin area.

2.6. Statistical analysis

Linear regression models (lm function, base package, R Core Team, 2024) were used to assess temporal trends in land-use proportions (%) as a function of year for each basin. Additional linear models were applied to evaluate the relationship between TN and OC concentrations (%).

Differences between the basins were assessed by one-way ANOVA (aov, base package, R Core Team, 2024) or Kruskal-Wallis test for non-parametric (kruskal.test, base package, R Core Team, 2024). Two-way ANOVA was applied to test the effects of sampling environment (estuary and mangrove) and seasonality (and their interaction) within each basin. For non-parametric, the effects were evaluated using a two-way approach based on the Aligned Rank Transform (ART) method (art, ARTool package, Kay et al., 2025), due to non-normality of residuals (Shapiro-Wilk test, $p < 0.05$). Post-hoc comparisons for significant interactions were performed using Tukey test (HSD.test, agricolae package, Mendiburu, 2023) and Dunn's test with Bonferroni adjustment (dunnTest, FSA package, Ogle et al., 2023; multcompLetters, multcompView package, Graves et al., 2024).

Isotopic biplot ($\delta^{13}C_{org}$ vs. $\delta^{15}N_{total}$ and $\delta^{13}C_{org}$ vs. $[C:N]_a$), were used to explore the distribution of sedimentary OM and to identify potential source endmembers. Endmember signatures were compiled from this study and previous literature. Marine OM signatures were defined as $\delta^{13}C_{org}$ and $\delta^{15}N_{total}$ were -20.1 ± 0.8 and 5.3 ± 3.1, respectively (Gatts et al., 2020; Serafim et al., 2023). Mangrove soil endmembers correspond to signatures measured in this study for both basin ($\delta^{13}C_{org} = -27.3 \pm 0.6$; $\delta^{15}N_{total} = 3.6 \pm 2.4$). For C4 vegetation $\delta^{13}C_{org}$ and $\delta^{15}N_{total}$ were -18.0 ± 0.7 and 4.6 ± 1.1, respectively (Ribas, 2012). Sewage endmembers followed Vezzone et al. (2021), who reported isotopic signatures ($\delta^{13}C_{org} = -23.5 \pm 0.7$; $\delta^{15}N_{total} = 5.9 \pm 0.5$) from a lagoon chronically impacted by sewage discharge, where mixing model results indicated ~50% OM contribution from untreated wastewater. Discrimination factors for C3, C4 and marine endmembers were retrieved from Serafim et al. (2023).

To estimate the relative contribution of potential OM sources to sedimentary pool, a Bayesian isotope mixing model was implemented (MixSIAR, MixSIAR package, Stock et al., 2018). Basin (CR and PSR) was included as a factor to estimate source contributions for each estuary separately. Convergence and model performance were assessed using standard diagnostics, including the Gelman–Rubin statistic, effective sample size, and visual inspection of trace plots and posterior density distributions. Source proportions were estimated using uniform Dirichlet priors ($\alpha = 1$). Model sensitivity to prior specification was evaluated by comparing results with weakly informative priors (α = 2,1,1,2). Posterior source contributions showed minimal variation between prior configurations, indicating that model outputs were primarily driven by isotopic data rather than prior assumptions.

Spearman's rank correlation (rcorr, Hmisc package, Harrell Jr., 2024) and Principal Component Analysis (PCA, FactoMineR package, Le et al., 2008) were used to evaluate the correlations among variables and to discriminate between the basins. Correlations were considered moderate between 0.4 and 0.7 and strong above 0.7. All data were standardized using decostand function by vegan package for PCA analysis (Oksanen et al., 2024).

Models' assumptions were validated using diagnostic plots (Altman and Krzywinski, 2016), and when necessary, data were transformed to meet ANOVA premises (linearity, normality, homoscedasticity, leverage), using a maximum likelihood function (boxcox, MASS package, Venables and Ripley, 2002). All analyses were conducted at a 95% confidence level. All statistics and analyses were performed using R version 4.4.0 (R Core Team, 2024).

3. Results

3.1. Land-use change between 1985 and 2024

The MapBiomas data, in both basins, classify the land cover and use into: forest (i.e., forest formation, savanna formation, mangrove, floodable forest, wooded sandbank vegetation, wetland, grassland formation, hypersaline tidal flat, rocky outcrop and herbaceous sandbank vegetation), farming (i.e., pasture, agriculture, forest plantation, mosaic of uses), non-vegetated (i.e., beach, dune and sand spot, urban area, mining, other non-vegetated areas, photovoltaic power plant) and water (i.e., aquaculture, river, lake and ocean; Table S3).

Table 1 and Fig. S1 summarize the temporal dynamics of land use and land cover between 1985 and 2024 in the drainage basins of the CR (Amazon Rainforest) and the PSR basin (Atlantic Rainforest). In the CR basin, natural vegetation predominated throughout the period but declined from 93.1% in 1985 to 54.1% in 2024 (−39.0 percentage points), mainly due to farming expansion that increased 37.6 percentage points over the same period. In the PSR basin, anthropogenic land use remained dominant above 70%, with farming occupying 72.0% in 1985 and slightly declining to 68.2% in 2024 (−3.8 percentage points). Natural cover showed a modest increase of 2.6 percentage points, largely explained by forest recovery from 24.4% to 26.9% (+2.5 percentage points).

Table 1
Land use and land cover in the past 40 years in the hydrographic basins of the Caeté River (Amazon Rainforest) and the Paraíba do Sul River (Atlantic Rainforest).

	Year				
Amazon Rainforest land use (%)	1985	1995	2005	2015	2024
Forest	91.81	83.11	66.79	56.20	52.83
Herbaceous and shrubby vegetation	0.20	0.14	0.05	0.05	0.05
Farming	6.31	14.86	30.35	40.74	43.90
Non-vegetated área	0.58	0.81	1.47	1.67	1.99
Water	1.10	1.08	1.35	1.34	1.23
Natural	93.1	84.3	68.2	57.6	54.1
Anthropogenic	6.9	15.7	31.8	42.4	45.9
Atlantic Rainforest land use (%)					
Forest	24.44	24.26	24.70	26.09	26.89
Herbaceous and shrubby vegetation	1.11	0.86	1.12	1.13	1.05
Farming	71.99	71.91	70.84	69.25	68.16
Non-vegetated área	1.27	1.60	1.95	2.24	2.48
Water	1.19	1.13	1.13	1.05	1.20
Natural	26.8	26.5	27.2	28.6	29.4
Anthropogenic	73.2	73.5	72.8	71.4	70.6

Beyond the general contrast between natural and anthropogenic land use, subclass analysis highlights finer patterns. In the CR basin (Table S4), forest cover declined by 38.6 percentage points while pasture expanded by 35.8 percentage points, representing a shift from forest-dominated to pasture-dominated land use. The PSR basin (Table S5) forest cover showed a slight recovery of 2.5 percentage points, but pasture remained dominant (>48%) throughout the years, likely linked to reduced mosaic uses through improved landscape distinction. Additionally, forest plantations expanded, and urban areas more than doubled, underscoring the intensification and diversification of anthropogenic pressures. These patterns are consistent with the strong and significant temporal trend of increasing anthropogenic land use in the CR basin (slope = 1.175, $R^2 = 0.94$, $p < 0.0001$) and a slight but significant declining trend in the PSR basin (slope = −0.075, $R^2 = 0.88$, $p < 0.0001$), indicating contrasting temporal trajectories of land use between basins.

3.2. Elemental and isotopic composition of organic matter

Fig. 2 illustrates the elemental and isotopic composition of surface sediment and mangrove soil from both estuarine zones, revealing distinct spatial and seasonal patterns between biomes, ecosystems, and hydrological periods.

Overall, PSR basin sediments showed higher OC concentration range compared to CR basin (from 0.02 to 5.4% [1.3 ± 1.5%], and from 0.04 to 1.3% [0.6 ± 0.6%], respectively), although the difference between the basins was not statistically significant (Fig. 2a; anova, $p > 0.05$). Seasonal variation was not significant when tested within each basin separately (Fig. 2b–c; $p > 0.05$). Differences were observed only between estuary and mangrove areas within basins (anova, $p < 0.0001$). In both basins, OC concentration was 3.9 and 4.7 times higher in mangroves areas compared to estuarine sediments for CR and PSR basins, respectively. TN concentration in the sediments from CR basin (from 0.03 to 3.5% [0.7 ± 1.1%]) was generally higher than PSR (from 0.02 to 0.6% [0.3 ± 0.2%]), but not statistically (Kruskal-Wallis, $p > 0.05$; Fig. 2d). In CR (Fig. 2e), TN concentration also showed a significant interaction between environment and season (anova, $p < 0.05$), with similarly high at mangrove and estuarine sites in the dry season, followed by a marked seasonal decline that was strongest at estuarine sites, where concentrations reached the lowest values during the rainy season. For PSR basin (Fig. 2f), only season had significant effects, with high values during the dry season (anova, $p < 0.05$). The $(C:N)_a$ ratio was generally lower in the PSR basin (10.9 ± 5.6), but not statistically

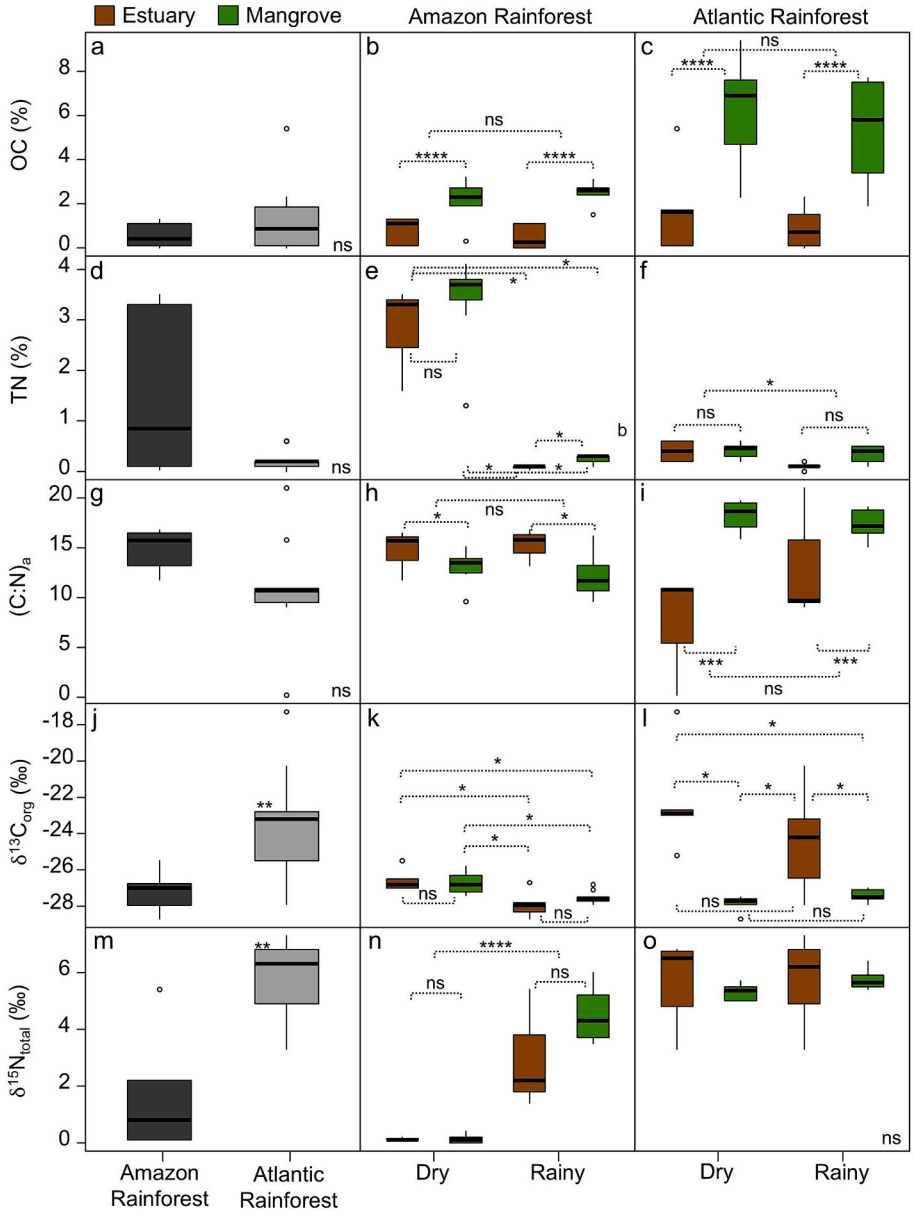

Fig. 2. Boxplots of OC and TN concentration (%), $\delta^{13}C_{org}$ (‰), $\delta^{15}N_{total}$ (‰), and $(C:N)_a$ ratios in surface sediments and soils from estuarine and mangrove environments in the CR and PSR (Amazon and Atlantic Rainforests, respectively). Comparisons are shown by biome (1st column) and season (2nd and 3rd column). Significant differences are indicated above or below the boxplots with brackets: **** $p < 0.0001$, *** $p < 0.001$, ** $p < 0.01$, * $p < 0.05$, ns = not significant. When the interaction between factors is not significant, brackets represent only main effects. When the interaction is significant, multiple comparisons are performed among all factor combinations. Gray boxplots correspond to estuarine sediments only, as they reflect basin-scale changes.

different (anova, $p > 0.05$) from CR basin (Fig. 2g; 15.0 ± 2.0). The $(C:N)_a$ showed no statistical difference (anova, $p > 0.05$) in seasonality for both basins (~13.0). In contrast, across environments (mangrove soils and estuarine sediments), $(C:N)_a$ values differed statistically, with higher values in mangrove soil (CR: 12.7 ± 1.8 and PSR: 17.8 ± 1.5) samples compared to estuarine sediments (CR: 15.0 ± 2.0 and PSR: 10.9 ± 5.5) for CR (Fig. 2h; anova, $p < 0.05$) and PSR (Fig. 2i; anova, $p < 0.001$) basin.

The sediment samples from CR basin were more ^{13}C-depleted (−27.3 ± 0.9‰), compared with PSR basin (−23.6 ± 2.9‰) (Kruskal-Wallis, $p < 0.01$; Fig. 2j). In the CR basin (Fig. 2k), $\delta^{13}C_{org}$ showed a significant interaction between environment and season (art, $p < 0.05$). Mangrove and estuary in dry season showed a significant ^{13}C-enrichement compared to both environment types in rainy season, but within season, environments did not show a significant difference. PSR basin (Fig. 2l), $\delta^{13}C_{org}$ also showed a significant interaction between environment and season (art, $p < 0.05$), with estuarine sites consistently more ^{13}C-enriched than mangroves, regardless of the season. Moreover, $\delta^{15}N_{total}$ showed moderate enrichment (5.6 ± 1.0‰; art, $p < 0.01$) in PSR basin compared with CR basin (2.1 ± 2.2‰; Fig. 2m). $\delta^{15}N_{total}$ values were significantly (art, $p < 0.0001$) more ^{15}N-depleted during the dry season (0.1 ± 0.1‰) compared to rainy season (4.1 ± 1.3‰) in CR basin (Fig. 2n), but for PSR basin (Fig. 2o), no statistical difference was observed (art, $p > 0.05$).

The biplots of $\delta^{13}C_{org}$ vs. $\delta^{15}N_{total}$ (Fig. 3a) allowed the identification of potential OM sources. Most CR samples clustered within the $\delta^{13}C_{org}$ and $\delta^{15}Nt_{otal}$ ranges typical of C_3 mangrove vegetation, indicating a predominantly autochthonous contribution. Conversely, PSR sediments exhibit a broader isotopic dispersion, with several samples plotting between the mangrove and sewage endmembers, and some approaching the marine range, probably the samples located further east (lower longitudes), reflecting the increasing marine influence along the

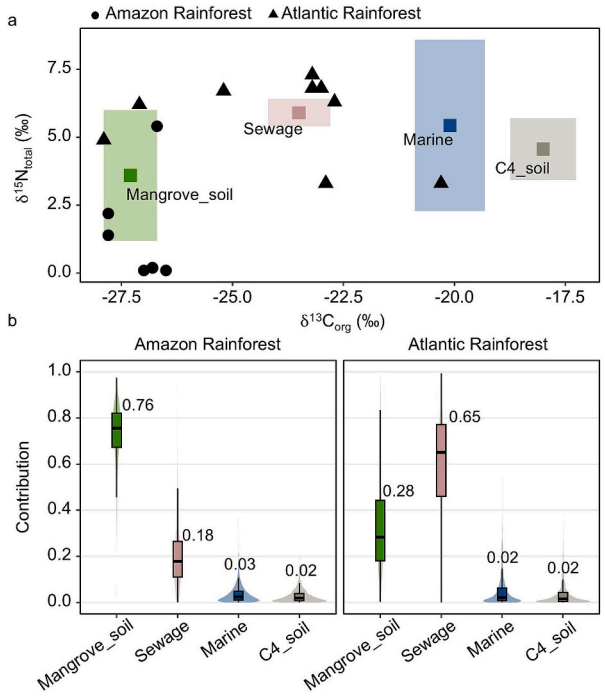

Fig. 3. Biplots of $\delta^{13}C_{org}$ (‰) vs. $\delta^{15}N_{total}$ (‰) (a) and posterior probability distributions of the proportional contribution of potential organic matter sources to sedimentary organic matter estimated using the Bayesian mixing model implemented in MixSIAR (b). Colored areas represent the mean and standard deviation of each end-member described in material and methods (e.g., C_3 and C_4 vegetation, sewage, marine sources). Violin plots represent the posterior density distributions of source contributions. The data were organized only with the results of $\delta^{13}C_{org}$ (‰) vs. $\delta^{15}N_{total}$ (‰).

estuarine gradient toward the river mouth.

The Bayesian mixing model indicated contrasting OM sources between the two estuarine systems. In the CR basin (Amazon Rainforest), mangrove-derived OM dominated sediment composition (median = 0.76), followed by sewage (0.18), while marine (0.03) and C_4-derived OM (0.02) contributed minimally. In contrast, in the PSR basin (Atlantic Rainforest), sewage represented the dominant source (0.65), whereas mangrove showed a secondary contribution (0.28). Contributions from marine and C_4 sources remained comparatively low in this basin (Fig. 3b). Although the PSR basin showed a tendency toward higher sewage contribution, the wide credible intervals of sewage and mangrove sources indicate and overlap, indicating an uncertainty in distinguishing these sources.

The relationship between TN and OC concentrations differed markedly between basins. In the PSR basin, TN increased linearly with OC ($R^2 = 0.95$, $p < 0.001$), indicating a strong covariation between both elements across the estuarine samples. In contrast, no significant relationship was observed in the CR basin ($R^2 = 0.04$, $p > 0.05$), suggesting a weaker coupling between TN and OC concentrations. These contrasting patterns indicate differences in the distribution and association of TN and OC between the two estuarine systems.

3.3. Organic pollutants distribution and sources

Among the analyzed compounds, several organochlorines and polybrominated substances exhibited concentrations below the analytical quantification limit (QL) of the method employed (Table S6). These include organochlorine pesticides (HCB, heptachlor and its epoxides, aldrin, isodrin, dieldrin, endrin, endosulfan I and II, methoxychlor, mirex, and chlordanes isomers) and PBDEs.

Correlation analysis for CR basin reveals that OC concentration is significantly positive moderate correlated with PAHs (sum of parental and alkylated PAHs), 16-PAHs, Alkyl-PAHs, high molecular weight (HMW)-PAHs, PCBs, DDTs and OCPs concentration (r_s = 0.58, 0.53, 0.51, 0.54, 0.52, 0.47 and 0.46, respectively). They are also positive and moderate correlated with the DDT concentrations (r_s = ~0.50), except low molecular weight (LMW)-PAHs. PSR basin also showed significantly and positively moderate to higher correlation among OC concentration and PAHs, 16-PAHs, Alkyl-PAHs, LMW-PAHs, HMW-PAHs, PCBs and OCPs concentration (r_s = 0.70, 0.68, 0.68, 0.65, 0.69, 0.54 and 0.45, respectively).

PCA results (Fig. S3) highlight the clear differences between the basins. PC1 explains 42% of the total variance and reflects industrial pollution and agricultural practices (PAHs, PCBs and DDTs) and is dominated by PSR estuarine samples. PC2 (20%) captures specifically agricultural contamination (OCPs, HCHs) and is associated with CR basin. Isotopic variables ($\delta^{13}C_{org}$ and $\delta^{15}N_{total}$) are aligned with PC1, showing enriched values in PSR and depleted values in CR, indicating that isotopic composition and contaminant concentrations co-vary between basins.

Fig. 4 shows the sum of each POP group in surface soil and sediment for CR and PSR basin. In general, CR basin (53.1 ± 48.6 ng g^{-1}) presents PAH concentrations 13.8 times lower (anova, $p < 0.0001$) than PSR basin (736.4 ± 880.3 ng g^{-1}; Fig. 4a). Fig. 4b exhibited a significant interaction between seasons and environment type in CR basin (anova, $p < 0.01$), with estuarine sediments during the rainy season presenting lower concentrations compared to sediments of dry season estuary and mangrove soils in both seasons. No differences were observed for PSR basin (Fig. 4c). Regarding HCH compounds, CR basin (0.7 ± 0.5 ng g^{-1}) showed concentrations more than 3 times higher (anova, $p < 0.0001$) compared PSR (0.2 ± 0.3 ng g^{-1}; Fig. 4d). Additionally, CR differed between environments and seasonality (Fig. 4e), with higher values in mangroves soils and dry season (anova, $p < 0.001$). In contrast, only seasonal effects were observed for PSR basin (anova, $p < 0.01$; Fig. 4f). As for DDT concentrations, PSR (0.3 ± 0.2 ng g^{-1}) was 1.7 times higher (anova, $p < 0.05$) than CR basin (0.1 ± 0.1 ng g^{-1}; Fig. 4g). No environmental or seasonal differences were observed within CR basin (Fig. 4h; anova, $p > 0.05$), while seasonal differences (anova, $p < 0.001$) were observed for PSR (Fig. 4i). For PCBs, PSR (1.5 ± 1.8 ng g^{-1}) presented concentrations more than 5 times higher (anova, $p < 0.0001$) compared to CR (0.3 ± 0.3 ng g^{-1}; Fig. 4j). Moreover, CR basin (Fig. 4k) statistically differs only between environments, with higher concentrations in mangrove soils (anova, $p < 0.01$). On the other hand, Fig. 4l showed significant interactions with only estuarine sites differing between seasonality (anova, $p < 0.01$).

The diagnostic ratio between parent PAHs illustrates the distribution of samples according to their potential sources in both basins (Fig. 5). The results based on the IP/IP + Bghi and Fl/Fl + Py ratios indicate a predominance of pyrogenic sources, but with different sources contribution, ranging from petroleum to sewage and biomass/coal combustion (Fl/Fl + Py). While samples from the PSR basin showed particularly strong signatures of sewage and biomass combustion, samples from CR basin plot closer to the petroleum combustion and petrogenic sources, indicating mixed inputs with a stronger influence of fossil fuel-related sources. In addition, the spatial pattern of the samples supports distinct combustion sources between both basins, with elevated DDT concentrations co-occurring with biomass combustion sources, especially in the PSR basin, suggesting the overlap of agricultural pesticides use and burning practices or shared transport.

A relatively high proportion of β-HCH was observed in the CR basin (59% and 62% during dry and rainy seasons, respectively), whereas HCHs in the PSR basin consisted entirely of the γ-HCH isomer. The β-HCH/(α + γ-HCH) ratio in CR samples was consistently above 0.5. Both basins showed mean (DDE + DDD)/DDT ratios above 0.50 (0.77 in CR and 0.85 in PSR), and DDD/DDE ratios lower than 1, except for one mangrove soil sample in each season. These ratios are commonly associated with aged residues and aerobic transformation processes reported

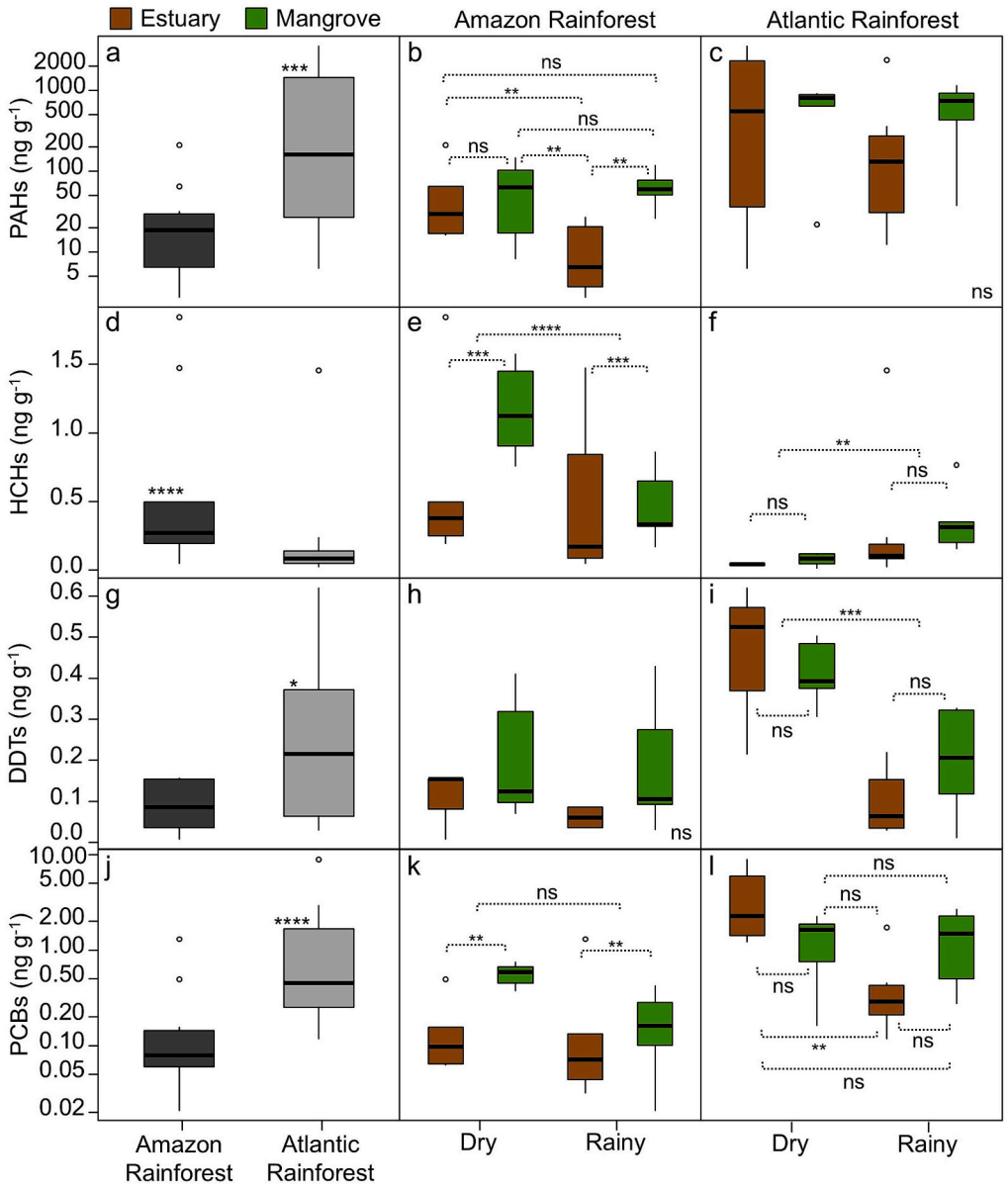

Fig. 4. Boxplots of PAHs, HCHs, DDTs and PCBs concentrations in surface sediments and soils from estuarine and mangrove environments in the CR and PSR (Amazon and Atlantic rainforest biomes, respectively). Comparisons are shown by biome (1st column) and season (2nd and 3rd column). Concentrations are given in ng g^{-1}. Significant differences are indicated above or below the boxplots with brackets: **** $p < 0.0001$, *** $p < 0.001$, ** $p < 0.01$, * $p < 0.05$, ns = not significant. When the interaction between factors is not significant, brackets represent only main effects. When the interaction is significant, multiple comparisons are performed among all factor combinations. A logarithmic scale was applied to the y-axis for PAHs and PCBs concentration for better visualization. Gray boxplots correspond to estuarine sediments only.

in the literature.

The basins also exhibit distinct average distributions of PCB congener classes, with the PSR basin showing percentages up to two times higher in penta-, hexa-, and hepta-chlorinated PCB compared to the CR basin (24.6, 25.6, 13.3 and 14.5, 12.7, 0.25% respectively). This pattern is consistent with our PCA results (Table S6), which highlight the association of higher-chlorinated PCBs (penta, hexa and hepta-CB) with the PSR basin (PC1: 63% of the total variance), suggesting stronger contributions from local and industrial sources, in contrast to the CR basin, where lower-chlorinated congeners prevail (tri-CBs, PC2: 13% of the total variance), indicative of long-range atmospheric transport.

4. Discussion

4.1. Deforestation legacies and urban pressures

The PSR (Atlantic Rainforest) and CR (Amazon Rainforest) basins exhibit distinct trajectories in land-use dynamics, face different anthropogenic pressures and their mangrove ecosystems exhibit contrasting biogeochemical responses, especially in OM composition. These differences reflect their distinct histories of human occupation. Land-use change affects estuarine sediments through multiple interconnected pathways. Alterations in vegetation cover and agricultural expansion modify the quantity and composition of OM exported from drainage basins, which can be traced using stable isotopes. At the same time, different anthropogenic activities, such as urbanization, agriculture, fire management and fossil fuel combustion, release organic pollutants that

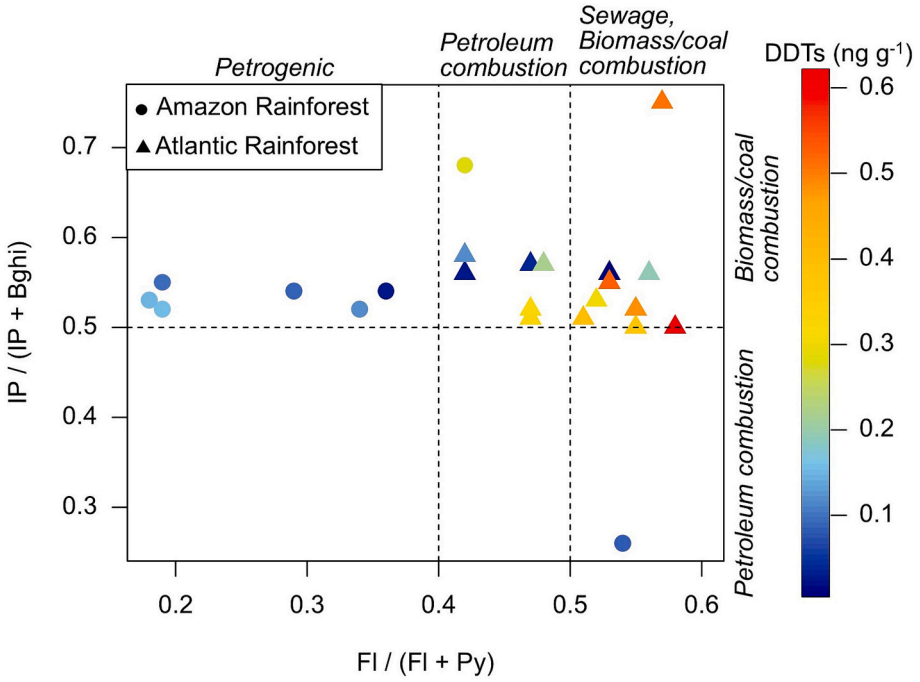

Fig. 5. PAH diagnostic ratios used to infer the sources of PAHs in the estuarine sediment samples from the Caeté River and Paraíba do Sul River colored by DDT. Many samples are not shown in the figure due to PAH concentrations below QL, preventing ratio calculations.

are preferentially transported and preserved in sediments due to their strong affinity for OM (Gao et al., 2012; Bianchi et al., 2018). Taken together, the co-variation between isotopic composition and contaminant concentrations observed in the PCA (Fig. S3) indicates that these proxies respond different processes occurring in the basins.

The Atlantic Rainforest, subject to land conversion since the 16th century (Dittmar et al., 2012; Solórzano et al., 2021; Pinto et al., 2023), has become Brazil's most industrialized and urbanized region. Within this biome, the PSR basin shows a long-standing and stable anthropogenic alteration, with over 70% of its area under human use for at least four decades. The remaining forest fragments are largely restricted to protected areas (Pinto et al., 2023). Although anthropogenic areas have slightly declined in recent decades, their persistence reflects the enduring legacy of historical degradation. Current pressures include deforestation (Lämmle et al., 2022; Pinto et al., 2023), industrial effluents (Pfeiffer et al., 1986; Tonhá et al., 2021), untreated sewage (AGEVAP, 2020), and coastal urban expansion, all contributing to global mangrove loss (Lämmle et al., 2022; Pinto et al., 2023). A linear increase in non-vegetated areas is evident (Fig. S1), particularly in urban zones (Table S5).

The CR basin represents a recent phase of intense land-use change, though not yet marked by extensive anthropogenic expansion. Driven by government-led colonization policies since the 1970s (Gorayeb et al., 2009, 2011), this basin exhibits active landscape recovery dynamics, contrasting sharply with the long-term degradation legacies of the PSR basin. Between 1985 and 2024, pastures expanded from 6 to 41%, reflecting farming intensification in northeastern Pará (Raiol et al., 2019), where forests were converted into pasture (Table S4). Coastal mangroves, however, show notable resilience, safeguarded by RESEX creation in the early 2000s (Gorayeb et al., 2011; Abdala et al., 2012; Pereira et al., 2021). These contrasting land-use trajectories provide a consistent framework to interpret the coupled variations in OM composition and contaminant signatures observed between basins.

4.2. Stable isotopes reflect land-use legacies

Overall, the elemental and isotopic composition of OM from surface sediments capture these contrasting land-use settings, providing a geochemical fingerprint of past and ongoing human influence (Fig. 2a, d, g, j and m).

Surface sediments from the Amazon and Atlantic Rainforest estuaries exhibited clear contrasts in their $\delta^{13}C_{org}$ and $\delta^{15}N_{total}$ values, while OC concentration remained relatively similar between both biomes (Fig. 2). The Amazon estuary sediments were more ^{13}C-depleted, indicating the dominance of C_3-plants as the main source. In contrast, the isotopic enrichment and clustering of PSR sediments near sewage, marine, and C_4-vegetation endmembers indicate a mixture of anthropogenic and natural inputs shaping the estuarine OM pool (do Prado et al., 2020; Serafim et al., 2023), consistent with the higher contaminant concentrations observed in this basin. Earlier studies in the Amazon basin reported $\delta^{13}C_{org}$ values between −27.5 and −25.8‰ for riverine sediments (Bouchez et al., 2014), consistent with C_3-vegetation, while a broader range, from −28.4 to −17.5‰, was found in the estuarine zone reflecting a mixture of terrestrial and marine sources (Cai et al., 1988). More detailed spatial assessments show that the most ^{13}C-depleted values (−31 to −27‰) occur in the inner estuary, while values gradually increase toward the estuary mouth, reaching approximately −25‰ (Weirich et al., 2025). More recently, Serafim et al. (2023) compared $\delta^{13}C_{org}$ values of coastal sediments from both biomes and found ^{13}C-enriched values for the Atlantic Rainforest (−22.6 ± 1.3‰) compared to the Amazon Rainforest (−25.0 ± 3.1‰) coastal sediments, with C_3-plants contributing to 35.6 and 51.3% to the OC concentration from the areas, respectively. Lower $(C:N)_a$ ratios in Atlantic Rainforest sediments further indicate greater contribution from primary producers and/or N-enriched anthropogenic sources, while higher ratios in the Amazon reflect more vascular plant-derived material. Overall, these isotopic patterns capture the stronger historical and ongoing anthropogenic imprint on the Atlantic Rainforest basin, while the Amazon system still retains a largely natural, vegetation-dominated composition.

Within the Amazon Rainforest, the CR basin, macrotidal dynamics strongly modulate the composition of OM (Fig. 2b, e, h, k and n; Fig. 3). While the elemental composition does not change over season, the $\delta^{13}C$ and $\delta^{15}N$ varies. During the dry season, low river discharge enhances tidal exchange and marine intrusion, with mangrove flats acting

predominantly as sediment importers (Asp et al., 2018). This hydrodynamic setting increases the relative marine contribution, leading to comparatively more ^{13}C-enriched and ^{15}N-depleted signatures in estuarine sediments and mangrove soils. Conversely, during the rainy season, mangrove OM export is intensified, with both dissolved and particulate fractions being exported in similar proportions (Dittmar et al., 2001). This enhanced export, together with increased surface runoff, results in more ^{13}C-depleted and ^{15}N-enriched values, consistent with anthropogenic inputs such as sewage discharge (Ribas, 2012; do Prado et al., 2020; Vezzone et al., 2021; Park et al., 2023). Effluent discharges reported by Monteiro et al. (2016) have shown that the CR estuary is affected, emphasizing sewage as an additional OM source. Despite upstream anthropogenic disturbances, the mangrove area has remained relatively stable over the last four decades (McLachlan et al., 2020; Table S4), displaying ^{13}C-depleted values controlled by the seasonality rather than progressive degradation. This pattern is further supported by the mixing model results, which indicate dominance of mangrove-derived OM in CR and sewage-derived OM in PSR.

The lack of relationship between TN and OC concentrations in the CR basin ($R^2 = 0.043$, $p > 0.05$) points to a biogeochemical decoupling potentially driven by post-depositional alteration and selective degradation (Gao et al., 2012; Guo et al., 2020). In such dynamic environments, nitrogen typically undergoes more rapid mineralization than carbon, leading to a loss of original biogenic signatures and a convergence of C/N ratios that may mask source identification. This decoupling might be also mediated by granulometric control, where the sediment texture governs the physical protection and preservation of OM (Craig, 1953; Thornton and McManus, 1994; Keil and Mayer, 2014; Bianchi et al., 2018). These findings align with the intense OM remineralization processes reported for the Amazon River plume by Serafim et al. (2023), reinforcing the role of mangroves as biogeochemical filters that attenuate upstream anthropogenic signals before they reach the ocean. In contrast, the PSR estuary, characterized by a microtidal regime, is more strongly influenced by river discharge (Shi et al., 2023). This hydrodynamic setting, combined with long-term land-use transformation, governs the isotopic and elemental composition of surface sediments in the PSR basin. The strong linear relationship between TN and OC ($R^2 = 0.95$) is consistent with a conservative mixing regime of refractory OM from distinct terrestrial and marine endmembers. This coupling suggests that distributions of TN and OC in the PSR basin are primarily governed by hydrodynamic transport and continental runoff, reflecting a pool dominated by organic nitrogen with limited contribution from mineral-bound nitrogen (Thornton and McManus, 1994; Keil and Mayer, 2014; Sartori et al., 2023).

In the Atlantic Rainforest, the PSR basin shows that spatial variability rather than seasonality drives the composition of OM in the estuarine sediment (Fig. 2c, d, i and l; Fig. 3). This lack of seasonality is likely explained by the decrease in runoff rates due to decades of human activities upstream and the decrease in river flow and precipitation rates, intensifying drought conditions during the dry season and reducing rainfall even in the rainy season (Oliveira et al., 2023). Distinct isotopic values between the mangrove and estuarine sites revealed contrasting OM composition: mangrove soils presented ^{13}C-depleted and ^{15}N-enriched values, reflecting their own contribution, while estuarine sediments had shown a different pattern, indicating a greater marine influence and likely reflecting the changes in the drainage basin. This spatial gradient highlights the efficient mixing and transformation of OM along the land-ocean continuum, controlled by geomorphology and limited tidal exchange. These findings are consistent with other southeastern Brazilian estuary under moderate hydrodynamic exchange and anthropogenic influence (Brandini et al., 2022). Nevertheless, it is important to note the wider range of $\delta^{13}C_{org}$ values observed during the rainy season (Fig. 2i). The more ^{13}C-depleted signatures likely reflect a greater contribution of historical C_3-plant material leached from deeper soils, combined with inputs from mangrove soils, as previously reported by Marques et al. (2017) and Serafim et al. (2023) for dissolved OM and coastal sediments, respectively.

Previous studies (e.g., Marques et al., 2017; Lizaga et al., 2021; Serafim et al., 2023, Dow et al., 2024) have shown that historical land-cover changes and continuous anthropogenic pressure have left a lasting isotopic legacy in estuarine sediments, often overriding natural sorting processes. Together, the isotopic and elemental composition patterns across both basins emphasize the diagnostic power of stable isotopes to disentangle natural and anthropogenic signals in tropical estuarine systems. While the estuarine sediments in the CR basin still reflect a system under dynamic yet partially buffered conditions, where mangrove productivity and tidal exchange mitigate the effects of land-use change upstream, in the PSR basin, reflects a higher persistent anthropogenic imprint, marked specially by $\delta^{13}C_{org}$ values as a result to the long-term anthropogenic pressure as well agricultural inputs.

4.3. Fingerprints of anthropogenic land-use through POPs

Extending the perspective on molecular markers of anthropogenic pressure, the distribution of POPs further illustrates how human activities are recorded in tropical estuarine sediments. While stable isotopes and elemental ratios primarily trace the origin and transformation of OM, POPs provide a complementary and more direct signal of industrial, agricultural, and urban emissions associated with land-use history. Because most POPs are hydrophobic, their environmental behavior is closely coupled with the transport and burial of OM. The co-occurrence of enriched isotopic signatures and elevated contaminant concentrations in PSR, as indicated by PCA (Fig. S3), reinforces this coupling between OM dynamics and pollutant accumulation (Hu et al., 2010).

Estuarine surface sediments from the Amazon and Atlantic Rainforests showed clear contrasts in POP concentrations (Fig. 4a, d, g, j), reflecting the distinct land-use trajectories of their drainage basins (Table 1). In the PSR estuary, PAH, DDT and PCB concentrations were markedly higher than in the CR estuary, consistent with the long-term legacy of land conversion, industrialization and urbanization. PAH concentrations in PSR (<QL – 2808.28 ng g^{-1}, 16-PAHs) exceeded values reported for several tropical estuaries, including the Subarnarekha (India, 181.2–511.3 ng g^{-1}; Ambade et al., 2021), Yellow River (China, 31.0–133.0 ng g^{-1}; Li et al., 2006), and surface sediments from Todos os Santos Bay (Brazil, 11.59–1825.35 ng g^{-1}; Nascimento et al., 2017), placing PSR among the most contaminated tropical estuarine systems. PCB concentrations were also higher in PSR (<DL – 8.94 ng g^{-1}), consistent with enrichment typically observed near industrial and urban centers (up to 4.78 ng g^{-}1; Souza et al., 2018a). Higher values have also been documented in other tropical estuaries in Brazil, such as the Santos estuary, with PCBs concentrations reaching 190.7 ng g^{-1} (Souza et al., 2018b).

In contrast, the CR estuary exhibited overall lower POP loads, but a contamination pattern dominated by OCPs. HCH concentrations were higher in the CR estuarine sediments (< QL – 1.84 ng g^{-1}) compared to PSR estuary (< QL – 1.43 ng g^{-1}), consistent with a stronger agricultural influence. This pattern aligns with the ongoing land-use change in CR basin, where rapid agricultural expansion (from 6.31 to 43.90%, from 1985 to 2024; Table 1) and limited regulatory control have shaped a contamination profile dominated by pesticides rather than industrial or combustion-derived pollutants. These levels are comparable to those reported for the Paranaguá Estuarine System (Brazil, < DL – 1.68 ng g^{-}1; Souza et al., 2018a). DDT concentrations in both estuaries (<QL – 0.43 in CR; <QL – 0.62 in PSR) were lower than those reported for Paranaguá (Brazil, <DL – 3.22 ng g;$^{-1}$ Souza et al., 2018a). Overall, the observed concentration ranges indicate that POP accumulation in PSR aligns with the upper end reported for tropical estuaries due to persistent industrial and urban influence, while CR basin reflects an agricultural-driven profile marked primarily by HCH contamination.

The predominance of HMW-PAHs in PSR basin may indicate fossil fuel combustion linked to urban centers and vehicular emissions (Maioli et al., 2011). Beyond these inputs, the dominance of combustion-derived

PAHs in our samples (Fig. 4), along with depleted $\delta^{13}C_{org}$ values (Fig. 2) and the documented use of agricultural fire management practices over the past four decades (Table 1), suggest a strong influence of both petroleum and biomass burning on sedimentary OM. Additionally, Fig. 5 reveals signal consistent with pyrogenic sources, although some diagnostic ratios (e.g., Fl/(Fl + Py)) can also reflect sewage/urban effluent inputs. Therefore, we interpret these signals as indicative of mixed combustion and/or sewage-related inputs rather than exclusively pyrogenic sources (Martins et al., 2010). Previous analyses of black carbon (BC), another proxy for biomass and fossil fuel incomplete combustion showed that historical burning of the Atlantic Rainforest and agricultural practices substantially increase the deposition of combustion products, which are transported from terrestrial systems to coastal environments along with the bulk OM (Dittmar et al., 2012; Marques et al., 2017; Serafim et al., 2023). In addition, the marked variability in DDT concentrations in the PSR indicates the influence of agricultural and pasture-management practices, such as pesticide application and biomass burning, which modulate the molecular markers observed in the system, consistent with high agricultural land use observed for this basin along the years. Distinctly, although the CR estuary presents an overall agricultural contamination profile, its PAH signatures indicate mixed combustion sources, with samples ranging from petrogenic to pyrogenic inputs (Fig. 5), likely reflecting contributions from localized seasonal field fire, small-scale boat traffic and fuel-oil spills (Yunker et al., 2002; Gorayeb et al., 2009).

HCH and DDT can also enter aquatic systems through surface runoff and sorption to particles (Parween et al., 2014). These OCPs were widely used in Brazilian agriculture and as a disease vector control from the 1940s until their complete ban in 2009, making Brazil a notable case on the global stage (Oliveira et al., 2016; Fernandes et al., 2020). Our results are consistent with this historical pattern in the CR basin, given the high proportion of β-HCH (~60%) and β-HCH/(α + γ-HCH) ratios above 0.5. β-HCH is the most stable, persistent and resistant isomer among the HCH (Yi et al., 2013). In the absence of significant recent inputs of technical HCH, the α-HCH and γ-HCH can be progressively transformed into β-HCH, increasing its relative proportion (Yang et al., 2010). In addition, technical HCH typically contains 5–14% β-HCH (Hu et al., 2010), thus the enrichment to ~60% is consistent with degradation and long-term environmental persistence of the other isomers (Hu et al., 2010; Tang et al., 2020). The predominance of β-HCH in the CR basin is consistent with the historical use of technical HCH, a low-cost formulation widely applied in Brazil, particularly in socioeconomically vulnerable regions such as Pará State, where limited access to more expensive lindane (γ-HCH) and weak regulatory enforcement likely favored its use (Gorayeb et al., 2009; Oliveira et al., 2016). PSR basin on the other hand, show only γ-HCH concentration, which is associated with lindane use (Yi et al., 2013).

Regarding the DDT class of compounds, the (DDE + DDD)/DDT ratios for both basins exceeded the threshold of 0.5, which is commonly interpreted as indicative of aged residues rather than recent inputs (Yang et al., 2010; Sreedevi and Harikumar, 2023). The predominance of DDE over DDD is generally associated with aerobic biodegradation processes (Oliveira et al., 2016). Such conditions may be favored by environmental factors such as tidal currents and sediment reworking, which enhance oxygen penetration and promote the persistence of DDE as the dominant metabolite.

PCBs are unintentionally formed and released during incomplete combustion of materials that contain chlorine; however, they are primarily associated with industrial activities and electrical applications (Nam et al., 2008; Mao et al., 2021). The observed differences in PCB concentration and congener distributions between the PSR and CR basins highlight these contrasting contamination patterns (Table S6). The PSR basin exhibits notably higher proportions and association with heavier PCBs suggesting a predominance of local/industrial sources (Mao et al., 2021), while the CR basin is dominated by lower-chlorinated congeners (tri-CBs), indicating inputs likely associated with long-range atmospheric transport (Nam et al., 2008; Mao et al., 2021). Such patterns reinforce the distinct anthropogenic signatures of each basin and the role of hydrodynamics in regulating contaminant deposition and export.

Hydrodynamic setting further modulates POPs behavior. Macrotidal dynamics in CR can promote resuspension and dilution, enhancing contaminant export to adjacent shelves, while the microtidal PSR estuary favors fine-sediment accumulation and long-term pollutant retention. The CR and PSR basins show the tendency to present lower concentrations for all POPs in estuarine sediments during the rainy season. However, no seasonal or spatial differences were observed for PAHs in the PSR basin, and DDTs and PCBs in CR basin suggesting a continuous input of mixed combustion sources, pesticides byproducts and atmospheric deposition, respectively. This pattern may be associated with persistent emissions from fossil fuel combustion, particularly in urban and industrial areas, as well as biomass burning linked to agricultural practices for PSR and pest control in agricultural, household and boat paint for CR basin (Maioli et al., 2011; Oliveira et al., 2016; Tang et al., 2020; Gurgatz et al., 2023). These anthropogenic molecular markers capture persistent inputs from combustion, agriculture, and industrial sources, reflecting distinct land-use legacies in the CR and PSR basins. Despite their relevance, such integrative approaches remain scarce in Brazilian estuarine research, underscoring the contribution of this study to understanding human impacts in tropical coastal environments.

Overall, the combined analysis of stable isotopes, organic contaminants, and land-use trajectories demonstrates that these systems exhibit coherent and coupled responses, where OM sources, contaminant inputs, and transport processes are mutually controlled by watershed-scale anthropogenic activities.

5. Conclusion

Our study highlights a clear contrast in the biogeochemical responses of Amazonia (CR) and Atlantic (PSR) Rainforest estuarine-mangrove systems under anthropogenic pressures. The CR basin, despite recent land-use changes, shows resilient mangroves attenuate upstream inputs, whereas the PSR basin reflects profound alteration from historical and ongoing human impacts. Stable isotopes and elemental ratios reveal contrasting sources and transformations of OM between the basins, while the distribution and composition of POPs provide complementary evidence of the dominant anthropogenic activities influencing each system. The co-occurrence of isotopic signatures and contaminant patterns, supported by multivariate analysis, demonstrates that these proxies respond to common watershed-scale processes linked to land-use trajectories. When interpreted, these proxies indicate that persistent pressures in the PSR basin, associated with intensive land use and urban emissions, override natural estuarine processes and produce a distinct geochemical imprint in surface sediments. In contrast, the CR basin, where mangroves remain largely preserved despite farming expansion, still exhibits OM signatures dominated by C3-derived inputs and comparatively lower contamination levels. POP signatures further distinguish these anthropogenic drivers: PAH ratios confirm pyrogenic sources in both basins, with PSR influenced by sewage/biomass burning, and fossil fuels, and CR with mixed combustion. PSR samples also show lindane and heavy PCB congeners from industrial activities, whereas CR sediments reflect historical HCH use and lighter PCB congeners consistent with diffuse atmospheric transport.

Together, these results indicate that OM composition and contaminant accumulation, are coupled and controlled not only by hydrodynamic conditions, but also reflects land-use history across basins. These findings underscore contrasting pollution patterns and the need for region-specific management. Overall, the combined use of isotopic tracers, molecular markers, and land-use reconstruction provides a coherent framework for understanding how different histories of human occupation shape OM dynamics and pollutant accumulation in tropical

estuarine systems, reinforces mangroves as biogeochemical barriers and informs future studies on human impacts in coastal systems.

CRediT authorship contribution statement

Échily Sartori: Writing – review & editing, Writing – original draft, Visualization, Validation, Methodology, Investigation, Formal analysis, Data curation, Conceptualization. **Cristiane dos Santos Vergilio:** Writing – review & editing, Supervision, Conceptualization. **Tassiana S. G. Serafim:** Writing – review & editing, Visualization, Formal analysis. **Diego Lacerda:** Writing – review & editing, Formal analysis. **Luiza Silva do Nascimento:** Investigation. **Pedro Vianna Gatts:** Writing – review & editing, Investigation. **Mariana Freitas:** Writing – review & editing, Investigation. **Jamile Tamer Nasser:** Validation, Methodology, Data curation. **Marcelo Gomes de Almeida:** Writing – review & editing, Validation, Methodology. **César C. Martins:** Writing – review & editing, Validation, Resources. **Nils E. Asp:** Writing – review & editing, Investigation. **Carlos Eduardo de Rezende:** Writing – review & editing, Validation, Supervision, Resources, Project administration, Investigation, Funding acquisition, Conceptualization.

Declaration of Generative AI and AI-assisted technologies in the writing process

All the text of the manuscript was initially written without AI. AI was used to correct some English formulations.

Funding statement

É. Sartori received grant from Coordenação de Aperfeiçoamento de Pessoal de Nível Superior - Brasil (88887.824229/2023-00) - Finance Code 001. É. Sartori and L. S. do Nascimento received scholarship from the CAPES/DAAD Probral Program, which supports international academic cooperation between Brazil and Germany (88887.989816/2024-00 and 88887.985811/2024-00). C.C. Martins thanks Conselho Nacional de Desenvolvimento Científico e Tecnológico (CNPq; grant code 310850/2020-7). Carlos E. de Rezende received grant from Fundação Carlos Chagas Filho de Amparo à Pesquisa do Estado do Rio de Janeiro (FAPERJ; Grant Code E-26/203.950/2024) and CNPq (Grant Code 310.260/2023-0 and 409.378/2022-4).

Declaration of competing interest

The authors declare that they have no known competing financial interests or personal relationships that could have appeared to influence the work reported in this paper.

Acknowledgments

We thank the Environmental Science Laboratory (Laboratório de Ciências Ambientais – LCA) of the Universidade Estadual do Norte Fluminense Darcy Ribeiro, the Marine Organic Chemistry Laboratory of the Universidade de São Paulo and the Coastal Geology Laboratory of the Universidade Federal do Pará, for providing infrastructure for sampling collection and further analysis. The final stage of this study was carried out with the participation of Carlos E De Rezende during his period as a fellow at Hanse-Wissenschaftskolleg – Institute for Advanced Study (HWK).

Appendix A. Supplementary data

Supplementary data to this article can be found online at https://doi.org/10.1016/j.marpolbul.2026.119899.

Data availability

Data will be made available on request.

References

Abdala, G., Saraiva, N., Wesley, F., 2012. Plano de Manejo da Reserva Extrativista Caeté-Taperaçu - VOLUME I - Diagnóstico da Unidade de Conservação. ICMBio, pp. 0–109.
AGEVAP - Associação Pro-Gestão das Águas da Bacia Hidrográfica do Rio Paraíba do Sul, 2020. Relatório sobre cenário ambiental 2020, 171p. https://www.ceivap.org.br/.
Altman, N., Krzywinski, M., 2016. Regression diagnostics. Nat. Methods 13 (5), 385–387. https://doi.org/10.1038/nmeth.385.
Álvarez, S., Valpassos, C.A.M. (Eds.), 2023. Alguns olhares do Sul: Antropologia, etnografia, e análise de conflitos e crises no século XXI. EDUENF, pp. 95–103.
Ambade, B., Sethi, S.S., Giri, B., Biswas, J.K., Bauddh, K., 2021. Characterization, behavior, and risk assessment of polycyclic aromatic hydrocarbons (PAHs) in the estuary sediments. Bull. Environ. Contam. Toxicol. 108 (2), 243–252. https://doi.org/10.1007/s00128-021-03393-3.
ANA, 2011. Estudos auxiliares para a gestão do risco de inundações. Bacia do Rio Paraíba do Sul - Setor Policial. Agência Nacional de Águas e Saneamento Básico.
Asp, N.E., Gomes, V.J.C., Schettini, C.A.F., Souza-Filho, P.W.M., Siegle, E., Ogston, A.S., Nittrouer, C.A., Silva, J.N.S., Nascimento, W.R., Souza, S.R., Pereira, L.C.C., Queiroz, M.C., 2018. Sediment dynamics of a tropical tide-dominated estuary: turbidity maximum, mangroves and the role of the Amazon River sediment load. Estuar. Coast. Shelf Sci. 214, 10–24. https://doi.org/10.1016/j.ecss.2018.09.004.
Bernardes, M.C., Martinelli, L.A., Krusche, A.V., Gudeman, J., Moreira, M., Victoria, R.L., Ometto, J.P.H.B., Ballester, M.V.R., Aufdenkampe, A.K., Richey, J.E., Hedges, J.I., 2004. Riverine organic matter composition as a function of land use changes, southwest Amazon. Ecol. Appl. 14, 263–279. https://doi.org/10.1890/01-6028.
Bianchi, T.S., Cui, X., Blair, N.E., Burdige, D.J., Eglinton, T.I., Galy, V., 2018. Centers of organic carbon burial and oxidation at the land-ocean interface. Org. Geochem. 115, 138–155. https://doi.org/10.1016/j.orggeochem.2017.09.008.
Bouchez, J., Galy, V., Hilton, R.G., Gaillardet, J., Moreira-Turcq, P., Pérez, M.A., France-Lanord, C., Maurice, L., 2014. Source, transport and fluxes of Amazon River particulate organic carbon: insights from river sediment depth-profiles. Geochim. Cosmochim. Acta 133, 280–298. https://doi.org/10.1016/j.gca.2014.02.032.
Bouillon, S., Borges, A.V., Castañeda-Moya, E., Diele, K., Dittmar, T., Duke, N.C., Kristensen, E., Lee, S.Y., Marchand, C., Middelburg, J.J., Rivera-Monroy, V.H., Smith III, T.J., Twilley, R.R., 2008. Mangrove production and carbon sinks: a revision of global budget estimates. Global Biogeochem. Cycles 22. https://doi.org/10.1029/2007gb003052.
Bouillon, S., Connolly, R.M., Gillikin, D.P., 2011. Use of stable isotopes to understand food webs and ecosystem functioning in estuaries. In: Treatise on Estuarine and Coastal Science, Vol. 7. Elsevier Inc., pp. 143–173. https://doi.org/10.1016/B978-0-12-374711-2.00711-7
Brandini, N., da Costa Machado, E., Sanders, C.J., Cotovicz Jr., L.C., Bernardes, M.C., Knoppers, B.A., 2022. Organic matter processing through an estuarine system: evidence from stable isotopes ($\delta^{13}C$ and $\delta^{15}N$) and molecular (lignin phenols) signatures. Estuar. Coast. Shelf Sci. 265, 107707. https://doi.org/10.1016/j.ecss.2021.107707.
Broggio, I.S., Silva-Junior, C.H.L., Nascimento, M.T., Villela, D.M., Aragão, L.E.O.C., 2024. Quantifying landscape fragmentation and forest carbon dynamics over 35 years in the Brazilian Atlantic Forest. *Environ. Res.* Lett. 19, 034047. https://doi.org/10.1088/1748-9326/ad281c.
Bunting, P., Rosenqvist, A., Hilarides, L., Lucas, R.M., Thomas, N., Tadono, T., Worthington, T.A., Spalding, M., Murray, N.J., Rebelo, L.-M., 2022. Global mangrove extent change 1996–2020: global mangrove watch version 3.0. Remote Sens. 14, 3657. https://doi.org/10.3390/rs14153657.
Cai, D.-L., Tan, F.C., Edmond, J.M., 1988. Sources and transport of particulate organic carbon in the Amazon River and estuary. Estuar. Coast. Shelf Sci. https://doi.org/10.1016/0272- 7714(88)90008-x.
Cornelissen, G., Gustafsson, Ö., Bucheli, T.D., Jonker, M.T.O., Koelmans, A.A., van Noort, P.C.M., 2005. Extensive sorption of organic compounds to black carbon, coal, and kerogen in sediments and soils: mechanisms and consequences for distribution, bioaccumulation, and biodegradation. Environ. Sci. Technol. 39 (18), 6881–6895. https://doi.org/10.1021/es050191b.
Cotovicz, L.C., Vidal, L.O., de Rezende, C.E., Bernardes, M.C., Knoppers, B.A., Sobrinho, R.L., Cardoso, R.P., Muniz, M., dos Anjos, R.M., Biehler, A., Abril, G., 2020. Carbon dioxide sources and sinks in the delta of the Paraíba do Sul River (southeastern Brazil) modulated by carbonate thermodynamics, gas exchange and ecosystem metabolism during estuarine mixin. Mar. Chem. 226. https://doi.org/10.1016/j.marchem.2020.103869.
Craig, H., 1953. The geochemistry of the stable carbon isotopes. Geochim. Cosmochim. Acta 3 (2–3), 53–92. https://doi.org/10.1016/0016-7037(53)90001-5.
Dittmar, T., Lara, R.J., Kattner, G., 2001. River or mangrove? Tracing major organic matter sources in tropical Brazilian coastal waters. Mar. Chem. 73. https://doi.org/10.1016/S0304-4203(00)00110-9.
Dittmar, T., de Rezende, C.E., Manecki, M., Niggemann, J., Coelho Ovalle, A.R., Stubbins, A., Bernardes, M.C., 2012. Continuous flux of dissolved black carbon from a vanished tropical forest biome. Nat. Geosci. 5 (9), 618–622. https://doi.org/10.1038/ngeo1541.
do Prado, M.R., de Carvalho, D.R., Alves, C.B.M., Moreira, M.Z., Pompeu, P.S., 2020. Convergent responses of fish belonging to different feeding guilds to sewage

pollution. Neotrop. Ichthyol. 18 (1). https://doi.org/10.1590/1982-0224-2019-0045.
Dow, S., Ouimet, W.B., Hren, M.T., 2024. Legacy impacts and recovery of δ15N, δ13C and C/N storage in soils due to historic land use. Anthropocene 46. https://doi.org/10.1016/j.ancene.2024.100435.
Eisma, D., Chen, S., Li, A., 1994. Tidal variations in suspended matter floc size in the Elbe river and Dollard estuaries. Neth. J. Aquat. Ecol. 28, 267–274. https://doi.org/10.1007/bf02334194.
Fernandes, C.L.F., Ramires, P.F., De Moura, R.R., Pohren, R. de S., Volcão, L.M., Junior, F.M.R. da S., 2020. Quais agrotóxicos estão contaminando os solos brasileiros? Res. Soc. Dev. 9 (3), e114932569. https://doi.org/10.33448/rsd-v9i3.2569.
Gao, X., Yang, Y., Wang, C., 2012. Geochemistry of organic carbon and nitrogen in surface sediments of coastal Bohai Bay inferred from their ratios and stable isotopic signatures. Mar. Pollut. Bull. 64 (6), 1148–1155. https://doi.org/10.1016/j.marpolbul.2012.03.028.
Gatts, P.V., Franco, M.A.L., Almeida, M.G., Zalmon, I.R., Di Beneditto, A.P.M., Costa, P.A.S., Rezende, C.E., 2020. The trophic ecology of marine catfishes in South-Eastern Brazil. J. Mar. Biol. Assoc. U. K. 100 (1), 133–142. https://doi.org/10.1017/S0025315419001164.
Gomes, V.J.C., Freitas, P.T.A., Asp, N.E., 2013. Dynamics and seasonality of the middle sector of a macrotidal estuary. J. Coast. Res. 165, 1140–1145. https://doi.org/10.2112/si65-193.1.
Gomes, P.R., Pestana, I.A., Viana, P.P., Almeida, M.G., Rezende, C.E., Souza, C.M.M., 2022. Effects of dams on As and Hg concentrations in three southeastern Brazil fluvial systems: ocean inputs, sources and seasonal dynamics among environmental compartments. Sci. Total Environ. 849. https://doi.org/10.1016/j.scitotenv.2022.157865.
Gorayeb, A., Lombardo, M.A., Pereira, L.C.C., 2009. Condições Ambientais em Áreas Urbanas da Bacia Hidrográfica do Rio Caeté – Amazônia Oriental - Brasil. Revista de Gestão Costeira Integrada 9 (2), 59–70. https://doi.org/10.5894/rgci117.
Gorayeb, A., Lombardo, M.A., Pereira, L.C.C., 2011. Natural conditions and environmental impacts in a coastal hydrographic Basin in the Brazilian Amazon. J. Coast. Res. 64 pg-pg. www.jstor.org/stable/26482393.
Graves, S., Piepho, H., Dorai-Raj, LSwhfS, 2024. multcompView: Visualizations of Paired Comparisons. R package version 0.1–10. https://CRAN.R-project.org/package=multcompView.
Guimarães, D.O., 2011. Condições Sócio-Ambientais da Bacia Hidrográfica do Rio Caeté (Pará, Brasil) [Thesis]. Universidade Federal do Pará. https://ppba.propesp.ufpa.br/ARQUIVOS/teses/2011/Tese_CondicoesSocioAmbientais.pdf.
Guo, Q., Wang, C., Wei, R., Zhu, G., Cui, M., Okolic, C.P., 2020. Qualitative and quantitative analysis of source for organic carbon and nitrogen in sediments of rivers and lakes based on stable isotopes. Ecotoxicol. Environ. Saf. 195, 110436. https://doi.org/10.1016/j.ecoenv.2020.110436.
Gurgatz, B.M., Garcia, M.R., Cabral, A.C., de Souza, A.C., Nagai, R.H., Figueira, R.C.L., de Mahiques, M.M., Martins, C.C., 2023. Polycyclic aromatic hydrocarbons in a natural heritage estuary influenced by anthropogenic activities in the South Atlantic: integrating multiple source apportionment approaches. Mar. Pollut. Bull. 188, 114678. https://doi.org/10.1016/j.marpolbul.2023.114678.
Harrell Jr., F., 2024. Hmisc: Harrell Miscellaneous. R package version 5.1–3. https://CRAN.R-project.org/package=Hmisc.
Hu, W., Lu, Y., Wang, T., Luo, W., Zhang, X., Geng, J., Wang, G., Shi, Y., Jiao, W., Chen, C., 2010. Factors affecting HCH and DDT in soils around watersheds of Beijing reservoirs, China. Environ. Geochem. Health 32, 85–94. https://doi.org/10.1007/s10653-009-9267-0.
Kay, M., Elkin, L., Higgins, J., Wobbrock, J., 2025. ARTool: Aligned Rank Transform for Nonparametric Factorial ANOVAs. doi:10.5281/zenodo.594511. https://doi.org/10.5281/zenodo.594511. R package version 0.11.2.
Keil, R.G., Mayer, L.M., 2014. Mineral matrices and organic matter. In: Treatise on Geochemistry. Elsevier, pp. 337–359. https://doi.org/10.1016/b978-0-08-095975-7.01024-x.
Lämmle, L., Perez Filho, A., Donadio, C., Arienzo, M., Ferrara, L., Santos, C. de J., Souza, A.O., 2022. Anthropogenic pressure on Hydrographic Basin and coastal Erosion in the Delta of Paraíba do Sul River, Southeast Brazil. J. Mar. Sci. Eng. 10 (11). https://doi.org/10.3390/jmse10111585.
Lapola, D.M., Martinelli, L.A., Peres, C.A., Ometto, J.P.H.B., Ferreira, M.E., Nobre, C.A., Aguiar, A.P.D., Bustamante, M.M.C., Cardoso, M.F., Costa, M.H., Joly, C.A., Leite, C. C., Moutinho, P., Sampaio, G., Strassburg, B.B.N., Vieira, I.C.G., 2014. Pervasive transition of the Brazilian land-use system. Nat. Clim. Chang. 4 (1), 27–35. https://doi.org/10.1038/nclimate2056.
Le, Sebastien, Josse, Julie, Husson, Francois, 2008. FactoMineR: an R package for multivariate analysis. J. Stat. Softw. 25 (1), 1–18. https://doi.org/10.18637/jss.v025.i01.
Li, G., Xia, X., Yang, Z., Wang, R., Voulvoulis, N., 2006. Distribution and sources of polycyclic aromatic hydrocarbons in the middle and lower reaches of the Yellow River, China. Environ. Pollut. 144 (3), 985–993. https://doi.org/10.1016/j.envpol.2006.01.047.
Li, D., Yan, J., Lu, Z., Chu, T., Li, J., Chu, T., 2023. Use of $\delta^{13}C$ and $\delta^{y}N$ as indicators to evaluate the influence of sewage on organic matter in the Zhangjiang mangrove–estuary ecosystem, southeastern China. Water 15 (20), 3660. https://doi.org/10.3390/w15203660.
Lizaga, I., Bodé, S., Gaspar, L., Latorre, B., Boeckx, P., Navas, A., 2021. Legacy of historic land cover changes on sediment provenance tracked with isotopic tracers in a Mediterranean agroforestry catchment. J. Environ. Manage. 288, 112291. https://doi.org/10.1016/j.jenvman.2021.112291.
Maioli, O.L.G., Rodrigues, K.C., Knoppers, B.A., Azevedo, D.A., 2011. Distribution and sources of aliphatic and polycyclic aromatic hydrocarbons in suspended particulate matter in water from two Brazilian estuarine systems. Cont. Shelf Res. 31 (10), 1116–1127. https://doi.org/10.1016/j.csr.2011.04.004.
Mao, S., Liu, S., Zhou, Y., An, Q., Zhou, X., Mao, Z., Wu, Y., Liu, W., 2021. The occurrence and sources of polychlorinated biphenyls (PCBs) in agricultural soils across China with an emphasis on unintentionally produced PCBs. Environ. Pollut. 271, 116171. https://doi.org/10.1016/j.envpol.2020.116171.
Marques, J.S.J., Dittmar, T., Niggemann, J., Almeida, M.G., Gomez-Saez, G.V., Rezende, C.E., 2017. Dissolved black carbon in the headwaters-to-ocean continuum of Paraíba Do Sul River, Brazil. Front. Earth Sci. 5. https://doi.org/10.3389/feart.2017.00011.
Martinelli, L.A., Nardoto, G.B., Soltangheisi, A., Reis, C.R.G., Abdalla-Filho, A.L., Camargo, P.B., Domingues, T.F., Faria, D., Figueira, A.M., Gomes, T.F., Lins, S.R.M., Mardegan, S.F., Mariano, E., Miatto, R.C., Moraes, R., Moreira, M.Z., Oliveira, R.S., Ometto, J.P.H.B., Santos, F.L.S., Vieira, S.A., 2020. Determining ecosystem functioning in Brazilian biomes through foliar carbon and nitrogen concentrations and stable isotope ratios. Biogeochemistry 154 (2), 405–423. https://doi.org/10.1007/s10533-020-00714-2.
Martins, C.C., Bícego, M.C., Rose, N.L., Taniguchi, S., Lourenço, R.A., Figueira, R.C.L., Mahiques, M.M., Montone, R.C., 2010. Historical record of polycyclic aromatic hydrocarbons (PAHs) and spheroidal carbonaceous particles (SCPs) in marine sediment cores from Admiralty Bay, King George Island, Antarctica. Environ. Pollut. 158, 192–200. https://doi.org/10.1016/j.envpol.2009.07.025.
McLachlan, R.L., Ogston, A.S., Asp, N.E., Fricke, A.T., Nittrouer, C.A., Gomes, V.J.C., 2020. Impacts of tidal-channel connectivity on transport asymmetry and sediment exchange with mangrove forests. Estuar. Coast. Shelf Sci. 233. https://doi.org/10.1016/j.ecss.2019.106524.
Mendiburu, F., 2023. agricolae: Statistical Procedures for Agricultural Research. R package version 1.3–7. https://CRAN.R-project.org/package=agricolae.
Monteiro, M.C., Jiménez, J.A., Pereira, L.C.C., 2016. Natural and human controls of water quality of an Amazon estuary (Caeté-PA, Brazil). Ocean Coast. Manag. 124, 42–52. https://doi.org/10.1016/j.ocecoaman.2016.01.014.
Nam, J.J., Gustafsson, O., Kurt-Karakus, P., Breivik, K., Steinnes, E., Jones, K.C., 2008. Relationships between organic matter, black carbon and persistent organic pollutants in European background soils: implications for sources and environmental fate. Environ. Pollut. 156 (3), 809–817. https://doi.org/10.1016/j.envpol.2008.05.027.
Nascimento, R.A., de Almeida, M., Escobar, N.C.F., Ferreira, S.L.C., Mortatti, J., Queiroz, A.F.S., 2017. Sources and distribution of polycyclic aromatic hydrocarbons (PAHs) and organic matter in surface sediments of an estuary under petroleum activity influence, Todos os Santos Bay, Brazil. Mar. Pollut. Bull. 119 (2), 223–230. https://doi.org/10.1016/j.marpolbul.2017.03.069.
Neves, A.D.O., Vilanova, M.R.N., 2021. Caracterização da seca histórica da década de 2010 na Bacia do Rio Paraíba do Sul, Estado de São Paulo, Brasil. Engenharia Sanitaria e Ambiental 26 (2), 339–349. https://doi.org/10.1590/s1413-415220190023.
Ogle, D.H., Doll, J.C., Wheeler, A.P., Dinno, A., 2023. FSA: Simple Fisheries stock Assessment methods. R package version 0.9.5. https://CRAN.R-project.org/package=FSA.
Oksanen, J., Simpson, G., Blanchet, F., Kindt, R., Legendre, P., Minchin, P., O'Hara, R., Solymos, P., Stevens, M., Szoecs, E., Wagner, H., Barbour, M., Bedward, M., Bolker, B., Borcard, D., Carvalho, G., Chirico, M., De Caceres, M., Durand, S., Evangelista, H., FitzJohn, R., Friendly, M., Furneaux, B., Hannigan, G., Hill, M., Lahti, L., McGlinn, D., Ouellette, M., Ribeiro Cunha, E., Smith, T., Stier, A., Ter Braak, C., Weedon, J., 2024. vegan: Community Ecology Package. R package version 2.6–6.1. https://CRAN.R-project.org/package=vegan.
Oliveira, A.H.B., Cavalcante, R.M., Duaví, W.C., Fernandes, G.M., Nascimento, R.F., Queiroz, M.E.L.R., Mendonça, K.V., 2016. The legacy of organochlorine pesticide usage in a tropical semi-arid region (Jaguaribe River, Ceará, Brazil): implications of the influence of sediment parameters on occurrence, distribution and fate. Sci. Total Environ. 542, 254–263. https://doi.org/10.1016/j.scitotenv.2015.10.058.
Oliveira, D.M., Carvalho, V.S.B., da Silva, B.C., Reboita, M.S., de Campos, B., 2023. Hydrological and precipitation extremes and trends over the Paraiba do Sul River basin, Brazil. Climate 11 (7), 138. https://doi.org/10.3390/cli11070138.
Ometto, J.P.H.B., Ehleringer, J.R., Domingues, T.F., Berry, J.A., Ishida, F.Y., Mazzi, E., Higuchi, N., Flanagan, L.B., Nardoto, G.B., Martinelli, L.A., 2006. The stable carbon and nitrogen isotopic composition of vegetation in tropical forests of the Amazon Basin, Brazil. Biogeochemistry 79 (1–2), 251–274. https://doi.org/10.1007/s10533-006-9008-8.
Park, H.J., Baek, N., Lim, S.S., Jeong, Y.J., Seo, B.S., Kwak, J.H., Lee, S.M., Yun, S.I., Kim, H.Y., Arshad, M.A., Choi, W.J., 2023. Coupling of δ13C and δ15N to understand soil organic matter sources and C and N cycling under different land-uses and management: A review and data analysis. Biol. Fertil. Soils 59 (5), 487–499. Springer Science and Business Media Deutschland GmbH. https://doi.org/10.1007/s00374-022-01668-3.
Parween, M., Ramanathan, A.L., Khillare, P.S., Raju, N.J., 2014. Persistence, variance and toxic levels of organochlorine pesticides in fluvial sediments and the role of black carbon in their retention. Environ. Sci. Pollut. Res. 21 (10), 6525–6546. https://doi.org/10.1007/s11356-014-2531-6.
Pereira, L.C.C., Sousa, N.S.S., Rodrigues, L.M.S., Monteiro, M.C., Silva, S.R.S., Oliveira, A.R.G., Dias, A.B.B., Costa, R.M., 2021. Effects of the lack of basic public sanitation on the water quality of the Caeté River estuary in northern Brazil. Ecohydrol. Hydrobiol. 21 (2), 299–314. https://doi.org/10.1016/j.ecohyd.2020.12.003.

Pfeiffer, W.C., Fiszman, M., Malm, O., Azcue, J.M., 1986. Heavy metal pollution in the Paraíba do sul river. Sci. Total Environ. 58, 73–79. https://doi.org/10.1016/0048-9697(86)90077-X.

Pinto, L.F.G., Ferreira, J., Berenguer, E., Rosa, M., 2023. Governance lessons from the Atlantic Forest to the conservation of the Amazon. Perspect. Ecol. Conserv. 21 (1), 1–5. https://doi.org/10.1016/J.PECON.2022.10.004.

R Core Team, 2024. R: A Language and Environment for Statistical Computing. R Foundation for Statistical Computing. https://www.R-project.org.

Raiol, L.L., Santos, D.C.R., dos Santos, D.S., da Silva, A.D.C., Júnior, J.F. da S., 2019. Uso e ocupação do solo e áreas de preservação permanente na Bacia Hidrográfica do Rio Caeté, Pará. Meio Ambiente em Foco, Vol. 10. Editora Poisson. https://doi.org/10.36229/978-85-7042-189-0.cap.13.

Ribas, L.M., 2012. *Caracterização de fontes de matéria orgânica do estuário do rio Paraíba do Sul, RJ, Brasil* [Thesis, Universidade Estadual do Norte Fluminense]. https://uenf.br/posgraduacao/ecologia-recursosnaturais/wp-content/uploads/sites/7/2013/11/Ligia-Macabu-Ribas-vers%C3%A3o-final.pdf.

Santos, F.R., Neves, P.A., Kim, B.S.M., Taniguchi, S., Lourenço, R.A., Timoszczuk, C.T., Bícego, M.C., 2020. Organic contaminants and trace metals in the western South Atlantic upper continental margin: anthropogenic influence on mud depocenters. Mar. Pollut. Bull. 154, 111087. https://doi.org/10.1016/j.marpolbul.2020.111087.

Santos-Andrade, M., Hatje, V., Arias-Ortiz, A., Patire, V.F., da Silva, L.A., 2021. Human disturbance drives loss of soil organic matter and changes its stability and sources in mangroves. Environ. Res. 202. https://doi.org/10.1016/j.envres.2021.111663.

Sartori, É., Vergilio, C.S., Gatts, P.V., Oliveira, B.C.V., Almeida, M.G., Thompson, F., Rezende, C.E., 2023. Trace metal concentration along the Brazilian coast: an assessment of the influence of the Doce River plume. Mar. Pollut. Bull. 188. https://doi.org/10.1016/j.marpolbul.2023.114640.

Serafim, T.S.G., Almeida, M.G., Thouzeau, G., Michaud, E., Niggemann, J., Dittmar, T., Seidel, M., Rezende, C.E., 2023. Land-use changes in Amazon and Atlantic rainforests modify organic matter and black carbon compositions transported from land to the coastal ocean. Sci. Total Environ. 878, 162917. https://doi.org/10.1016/j.scitotenv.2023.162917.

Shi, L., Ortals, C., Valle-Levinson, A., Olabarrieta, M., 2023. Influence of river discharge on tidal and subtidal flows in a microtidal estuary: implication on velocity asymmetries. Adv. Water Resour. 177, 104446. https://doi.org/10.1016/j.advwatres.2023.104446.

Solórzano, A., Brasil, L.S.C.A., Oliveira, R.R., 2021. The Atlantic Forest ecological history: from pre-colonial times to the Anthropocene. In: The Atlantic Forest: History, Biodiversity, Threats and Opportunities of the Mega-Diverse Forest. Springer, Cham, pp. 25–44. https://doi.org/10.1007/978-3-030-55322-7_2.

Souza, A.C., Combi, T., da Silva, J., Martins, C.C., 2018a. Occurrence of halogenated organic contaminants in estuarine sediments from a biosphere reserve in southern Atlantic. Mar. Pollut. Bull. 133, 436–441. https://doi.org/10.1016/j.marpolbul.2018.05.052.

Souza, A.C., Taniguchi, S., Lopes Figueira, R.C., Montone, R.C., Caruso Bícego, M., Martins, C.C., 2018b. Historical records and spatial distribution of high hazard PCBs levels in sediments around a large south American industrial coastal area (Santos estuary, Brazil). J. Hazard. Mater. 360, 428–435. https://doi.org/10.1016/j.jhazmat.2018.08.041.

Sreedevi, M.A., Harikumar, P.S., 2023. Occurrence, distribution, and ecological risk of heavy metals and persistent organic pollutants (OCPs, PCBs, and PAHs) in surface sediments of the Ashtamudi wetland, south-west coast of India. Reg. Stud. Mar. Sci. 64, 103044. https://doi.org/10.1016/j.rsma.2023.103044.

Stock, B.C., Jackson, A.L., Ward, E.J., Parnell, A.C., Phillips, D.L., Semmens, B.X., 2018. Analyzing mixing systems using a new generation of Bayesian tracer mixing models. PeerJ 6, e5096. https://doi.org/10.7717/peerj.5096.

Tang, D., Liu, X., He, H., Cui, Z., Gan, H., Xia, Z., 2020. Distribution, sources and ecological risks of organochlorine compounds (DDTs, HCHs and PCBs) in surface sediments from the Pearl River estuary, China. Mar. Pollut. Bull. 152, 110942. https://doi.org/10.1016/j.marpolbul.2020.110942.

Thornton, S.F., McManus, J., 1994. Application of organic carbon and nitrogen stable isotope and C/N ratios as source indicatiors of organic matter provenance in estuarine systems: evidence from the Tay Estuary, Scotland. Estuar. Coast. Shelf Sci. 38, 219–233.

Tonhá, M.S., Araújo, D.F., Araújo, R., Cunha, B.C.A., Machado, W., Portela, J.F., PR Souza, J., Carvalho, H.K., Dantas, E.L., Roig, H.L., Seyler, P., Garnier, J., 2021. Trace metal dynamics in an industrialized Brazilian river: a combined application of Zn isotopes, geochemical partitioning, and multivariate statistics. Journal of Environmental Sciences 101, 313–325. https://doi.org/10.1016/j.jes.2020.08.027.

Turubanova, S., Potapov, P.V., Tyukavina, A., Hansen, M.C., 2018. Ongoing primary forest loss in Brazil, Democratic Republic of the Congo, and Indonesia. Environ. Res. Lett. 13 (7), 074028. https://doi.org/10.1088/1748-9326/AACD1C.

Venables, W.N., Ripley, B.D., 2002. Modern Applied Statistics with S, Fourth edition. Springer, New York. ISBN 0-387-95457-0.

Vezzone, M., Meigikos dos Anjos, R., Gonçalves Cesar, R., Muniz, M., Cardoso, R., Paulo Felizardo, J., Vasconcelos, D., Polivanov, H., Vezzone mvezzone, M., 2021. Using stable isotopes to discriminate anthropogenic impacts of the sedimentary organic matter pollution in the Rodrigo de Freitas Lagoon (RJ, Brazil). Environ. Sci. Pollut. Res. Int. https://doi.org/10.1007/s11356-020-10835-8.

Ward, N.D., Bianchi, T.S., Medeiros, P.M., Seidel, M., Richey, J.E., Keil, R.G., Sawakuchi, H.O., 2017. Where carbon Goes when water flows: carbon cycling across the aquatic continuum. Front. Mar. Sci. 4. https://doi.org/10.3389/fmars.2017.00007.

Weirich, Y.S.V., Rezende, C.E., Souza, F.M., Santos, V.F., Martins, C.C., 2025. Unraveling sedimentary organic matter in the Oiapoque estuarine-marine ecosystem: insights from elemental composition and isotopic fingerprints on the Amazon coast. Mar. Chem. 273, 104565. https://doi.org/10.1016/j.marchem.2025.104565.

Yang, H., Xue, B., Yu, P., Zhou, S., Liu, W., 2010. Residues and enantiomeric profiling of organochlorine pesticides in sediments from Yueqing Bay and Sanmen Bay, East China Sea. Chemosphere 80 (6), 652–659. https://doi.org/10.1016/j.chemosphere.2010.04.052.

Yi, Z., Zheng, L., Guo, P., Bi, J., 2013. Distribution of α-, β-, γ-, and δ-hexachlorocyclohexane in soil–plant–air system in a tea garden. Ecotoxicol. Environ. Saf. 91, 156–161. https://doi.org/10.1016/j.ecoenv.2013.01.024.

Yunker, M.B., Macdonald, R.W., Vingarzan, R., Mitchell, R.H., Goyette, D., Sylvestre, S., 2002. PAHs in the Fraser River basin: a critical appraisal of PAH ratios as indicators of PAH source and composition. Org. Geochem. 33, 489–515. https://doi.org/10.1016/s0146-6380(02)00002-5.

Zhao, J., Zhang, L., Zhang, Y., Yu, Q., Luo, S., 2024. Lipid biomarker evidences of natural and anthropogenic organic matter inputs in sediments from the eastern Sunda Shelf in the southern South China Sea. Cont. Shelf Res. 275, 105184. https://doi.org/10.1016/j.csr.2024.105184.